Viewing stomata in action: Autonomous *in planta* imaging of individual stomatal movement

Tomas E. van den Berg[i1], Remco. G. P. Sanders[1], Elias Kaiser[ii2] and Jurriaan Schmitz[1]

[1]Integrated Devices and Systems, University of Twente, Drienerlolaan 5, 7522 NB Enschede, The Netherlands

[2] Horticulture and Product Physiology, Department of Plant Sciences, Wageningen University & Research, Wageningen 6708PB, The Netherlands

keywords: stomata, water-use efficiency, chrysanthemum, stomatal aperture kinetics, microscopy, photosynthesis, maize, fluctuating light, stomatal movement

Summary

Stomata regulate plant gas exchange under changing environments, but observations of the dynamics of single stomata *in planta* are sparse. We developed a compact microscope system that can measure the kinetics of tens of stomata *in planta* simultaneously, with sub-minute time resolution. Dark field imaging with green light was used to create 3D stacks from which 2D surface projection were constructed to resolve stomatal apertures within the field of view.

Stomatal dynamics of *Chrysanthemum morifolium (*Chrysanthemum*)* and *Zea Mays* (Maize) under dynamically changing light intensity were categorized, and a kinetic model was fitted to the data for quantitative comparison. In addition, we also resolved dynamics of the surface position of the leaf, related to dynamics of leaf thickness or bending.

Maize stomata oscillated frequently between open and closed states under constant growth light and these oscillating stomata responded

faster to changes in light than non-oscillating stomata at the same aperture.

The slow closure of Chrysanthemum stomata reduced water use efficiency (WUE). Over 50% showed delayed or partial closure, leading to unnecessarily large apertures after reduced light. Stomata with larger apertures had more lag and similar closure speeds compared to those with smaller apertures and lag, further reducing WUE. In contrast, maize stomata with larger apertures closed faster, with no lag.

In conclusion, our new system enables fine mapping of the heterogeneity of movement in neighboring stomata, providing new insights on the relations between stomatal dimensions, relative position and aperture changes under fluctuating light intensity.

Introduction

Due to climate-change driven increases in air temperature and Vapor Pressure Deficit (VPD) (Novick *et al.*, 2016) and decreased rainfall in many agricultural areas (Dore, 2005), future crop yields are coming under pressure. Adaptation of agriculture is therefore essential to maintain food security for an increasing world population (Anderson, Bayer and Edwards, 2020). A pillar for agricultural adaptation is the development of varieties with increased water use efficiency (WUE). To achieve this, we need to thoroughly understand the role that stomata play in plant WUE, which is often defined as the rate of photosynthesis divided by the rate of transpiration (Bertolino, Caine and Gray, 2019; Buckley, 2019; Lawson and Vialet-Chabrand, 2019; Nadal and Flexas, 2019), to breed for stomatal traits underlying high WUE.

Stomata are the microscopic pores on plant leaves that regulate their gas exchange, by dynamically opening and closing in

response to environmental and intrinsic stimuli (Lawson and Matthews, 2020). Their dynamic behavior (Lawson and Vialet-Chabrand, 2019), morphology and density (Bertolino, Caine and Gray, 2019; Duursma *et al.*, 2019) are important for WUE. Stomatal conductance to CO_2 diffusion into the leaf facilitates photosynthetic CO_2 fixation in the mesophyll, and stomatal movement broadly aims to balance the CO_2 taken up by photosynthesis with the water vapor lost through transpiration. Light intensity changes of ~25-50 fold on single leaves are frequent in the crop growth environment (Kaiser, Morales and Harbinson, 2018). When the light intensity drops, the photosynthetic demand for CO_2 decreases near-instantaneously, while stomatal closure proceeds much more slowly. Hence, stomata that at that moment are open more than strictly necessary for CO_2 demand, waste water through unnecessary transpiration. Fast-closing stomata are thus more water use efficient (Papanatsiou *et al.*, 2019; Horaruang *et al.*, 2022).

An increase in light intensity quickly causes photosynthetic demand for CO_2 to increase, as biochemical limitations are lifted in the first minutes of photosynthetic induction (Sakoda *et al.*, 2021). To meet this demand for CO_2, stomata need to open to increase the rate of diffusion of CO_2, leading to a transient limitation of photosynthesis while opening. Transient limitations of photosynthesis in shade-sun transitions may cost an estimated 10-40% of potential crop CO_2 assimilation (Long *et al.*, 2022).

Stomatal dynamics are most frequently studied using leaf-level gas exchange measurements and are then related to static microscopic observations of e.g. leaf epidermal peels to stomatal density and morphology. Alternatively, dynamic behaviour of individual stomata has been studied on epidermal peels, missing the interaction with the mesophyll (Weyers and Travis, 1981; Blatt, 1987; Pantaleno *et al.*, 2024). Measurements of bulk stomatal behavior, such as those of leaf gas exchange, hide the variation between individual stomata (Kaiser and Paoletti, 2014), and studies that have resolved individual stomatal dynamics *in planta* are relatively rare (Kaiser and Kappen, 1997, 2000,

2001; Kaiser, 2009; Grantz, Zinsmeister and Burkhardt, 2018). Moreover, minimizing the boundary layer of still air surrounding the leaf, as is common in gas exchange measurements (Busch *et al.*, 2024), limits the study of stomatal behavior under frequently occurring natural conditions, when a significant boundary layer is present (Pattey *et al.*, 1991; Goldstein *et al.*, 1995). Information is lacking on how local morphology and density influence the dynamics of individual stomata. Such characteristics could lead to a better understanding of stomatal control and breeding targets for WUE and yield (Haworth *et al.*, 2021). Additionally, it is essential to study such characteristics in the field, e.g. to understand how plants with altered stomatal characteristics respond to multiple stresses in different developmental phases (Bertolino, Caine and Gray, 2019).

Here, we describe a newly developed portable microscope, which can measure the opening and closure of tens of individual stomata simultaneously in the growth environment. Our method innovates on previous methods by selective use of green light for imaging and blue and red light as actinic light. In addition, we imaged the entire field of view (FOV) of the surface of the leaf, by creating large image stacks that were used to create leaf surface projections, in contrast to autofocus onto single pores (Kaiser and Kappen, 1997; Grantz, Zinsmeister and Burkhardt, 2018). This enabled us to relate stomatal dynamics to characteristics such as 'the Voronoi area', the leaf area with the shortest path length to a given stoma. Acquisition and analyses were largely automated, facilitating easy measurements. We demonstrated our method on leaves of Chrysanthemum *,* a greenhouse crop with elliptic stomata whose stomatal behavior can limit vase life (Fanourakis *et al.*, 2021) and the rate of photosynthetic induction (Zhang *et al.*, 2022) and the staple crop Maize with dumbbell stomata.

Materials and Methods

Microscope

The design of our microscope focused on obtaining images with sub-micrometer resolution at different focus planes to resolve the 3D surface of the leaf with sub-minute time resolution. Additionally, the design aimed to be minimally invasive to the leaf's microclimate.

We achieved high optical resolution with high quality optics (plan APO series objectives, Mitutoyo, Japan and TTL200-S8 tube lens, Thorlabs, United States), verified with a calibration target (micro V2, Opto, Germany). The 20x objective (NA 0.42) enabled imaging of ~0.45 mm^2 (722x625 µm) of the leaf's surface. High time resolution of stacks of 100 images spaced 1 µm apart on the axis perpendicular to the imaging plane (z-axis; below the 1.6 µm depth of focus of the microscope objective) was achieved with a fast and accurate step motor (Z812, Thorlabs, United States, range of 12 mm, 0.2 µm precision), which was controlled with autofocus software and a CMOS camera (BFS-U3-244S8M-C; Teledyne-FLIR, Wilsonville, OR, USA). The high sensitivity of the camera and on-camera pixel binning (2x2) allowed us to achieve high quality images at a relatively low light intensity (50-75 µmol photons m^{-2} s^{-1}) and short integration time (400 ± 100 ms). The use of long working distance objectives (20 mm) and leaf clips that were laser-cut from transparent polycarbonate with 2 mm neoprene cushions allowed us to image the leaf with low obstruction to air flow and light. Imaging made use of green light only (Effiring 525 nm; Effilux, Hürth-Efferen, Germany, for Chrysanthemum, SL-3500, PSI, Czech Republic, for Maize) by filtering light that passed through the objective with a bandpass filter (FB550-40, 550 ± 8 nm, FWHM 40 ± 8 nm; Thorlabs, Newton, NJ, USA). Monochromatic light was chosen, because it boosted image quality by limiting chromatic aberrations. Green light was selected because of its high reflectance by and transmission through the leaf, higher optical resolution compared to near-infrared radiation, and a maximum sensitivity of the camera in the green waveband.

Optimization of imaging light was achieved before each automated measurement, by manually changing the emission angle and diffusivity (by changing the opacity of the window) of the imaging light. Blue-red actinic illumination was emitted by a custom-built LED lamp for Chrysanthemum (444/661 nm, 20/12 nm FWHM, 52/48%; Seven steps to heaven, the Netherlands) and by an RGB LED panel (SL-3500, PSI, Czech Republic) for Maize. Imaging could be done in brightfield or darkfield (with the green ring light above the leaf and blue-red light passing through the central hole of the green LED ring for Chrysanthemum). Maize and Chrysanthemum were imaged in darkfield. Both actinic and imaging light were controlled via LabVIEW (2018, National Instruments, Austin, TX, USA) and intensity calibrated at the leaf position with a photosynthetically active radiation (PAR) quantum sensor (Li-190R; Li-Cor Biosciences, Lincoln, NE, USA). Leaves were clamped in the microscope leaf holder that was equipped with embedded magnets at four contact points. The portable microscope was mounted on a tripod (Fig. 1). PAR intensity fluctuations during the measurement were recorded with a leaf clip holder (2020-B) connected to a portable fluorometer (MINI-PAM; Walz, Effeltrich, Germany).

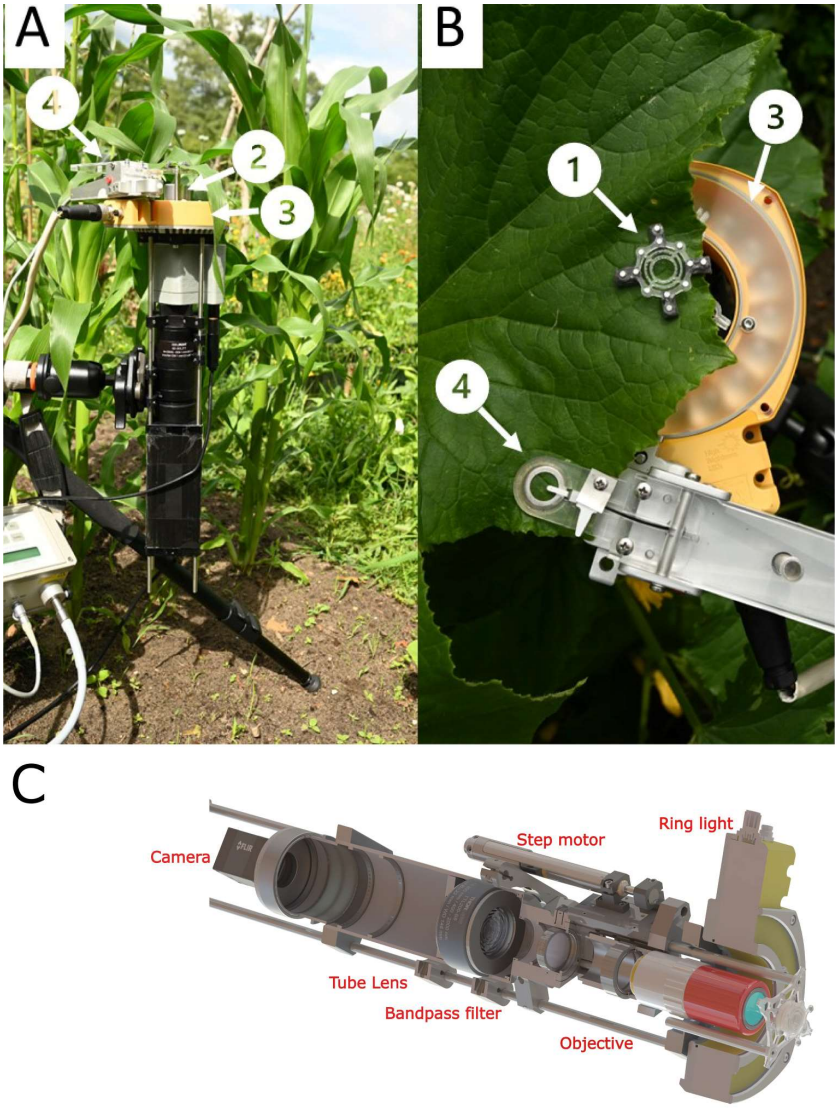

Figure 1. Overview of the leaf microscope. Example of the microscope A. Side view of the entire microscope with a leaf of maize (Maize) clamped in the holder. B. Top view of a leaf of cucumber (Cucumis sativa) clamped in the holder. The leaf clip (1) holds the leaf in place via magnets embedded in the polycarbonate framework. Neoprene cushions ensure a minimal effect of the clamping on the surface of the leaf. The microscope objective (2) can focus automatically, and the ring light (3) provides illumination for microscopy. The leaf clip from the mini-PAM (4) records PAR, ambient air temperature (A) or leaf temperature (B). C. Visualization of the layout with the most important components. Note that in this example, the green ring light is installed for brightfield imaging.

Software

Acquisition

The data acquisition workflow was developed in Labview. Camera settings, number of images per stack with different focus planes on the z-axis (z-stack) and stack depth, imaging and light intensity and

195 duration, as well as autofocus settings that determined the position
196 of the stack's center (methods: Roberts, Sobel, Gradient (Lthi *et al.*,
197 2010)) were controlled via the interface in Labview. Full protocol files
198 with imaging, light timing as well as light intensity settings can be
199 loaded into the software with a graphical user interface for inspection.

200 ## Analyses

201 Acquired z-stack images, in 16bit TIFF format belonging to each z-
202 stack, were processed in several stages (Fig. 2) using Fiji open-source
203 software (Schindelin et al., 2012). Images were denoised (despeckle
204 and outlier removal), normalized for intensity (enhance contrast,
205 normalize) and aligned (SIFT linear stack alignment (Lowe, 2004))
206 (SM-Methods-Analyses). SM movie 1 is an example of a processed
207 image stack. Next, the plugin "extended depth of field" (Forster *et al.*,
208 2004) was used to generate a focus projection of the leaf surface,
209 reducing the stack to a single image per timepoint (SM-Methods-
210 Analyses). All timepoint focus projections were then stacked again to
211 generate a video of the entire experiment that was again aligned to
212 adjust for x-y axis movements of the leaf during the experiment (SIFT
213 linear stack alignment). This stack was then cropped, to include only
214 the area that was within view during the entire experiment, shadow
215 corrected using the pseudo flat field correction in the BioVoxxel plugin
216 (Brocher, 2015) and contrast enhanced using the contrast limited
217 adaptive histogram equalization (CLAHE) algorithm (SM-Methods-
218 Analyses) (Reza, 2004) (Fig. 3 A-C). SM movie 2 is an example of a
219 processed video from an entire experiment, while SM movie 3 is a
220 zoomed-in version of a single stoma. Auto thresholding was done in
221 Percentile mode (Doyle, 1962) for Chrysanthemum (Fig. 3D) and in
222 Berndsen mode (Sezgin and Sankur, 2004) for Maize, as it generated
223 the best segmentation of open pores (SM-Methods-Analyses). SM
224 movie 4 is SM movie 3 after thresholding. Stomata in the stack were
225 manually selected with the elliptical (Chrysanthemum) or rectangular
226 (Maize) selection tool and added in the region of interest (ROI)
227 manager (ImageJ). Pore areas were then quantified via the 'analyse
228 particles' menu for each stoma in the ROI manager, to quantify pore

area and to generate masks for visual inspection of pore shapes for the entire experiment (Fig 3D). SM video 5 shows the masks generated from the stoma in SM videos 3 and 4.

Kinetics of stomatal aperture changes were loaded into Origin (OriginLab Corporation, Nothampton, MA, USA) and data of opening and closing were fitted separately with the model developed for kinetics of stomatal conductance (Vialet-Chabrand, Dreyer and Brendel, 2013):

$$A(t) = (A_{max-i} - A_{0-i})\, e^{-e^{(\frac{\lambda_i - t}{k_i} - 1)}} + A_{0-i}. \qquad \text{(Eqn. 1)}$$

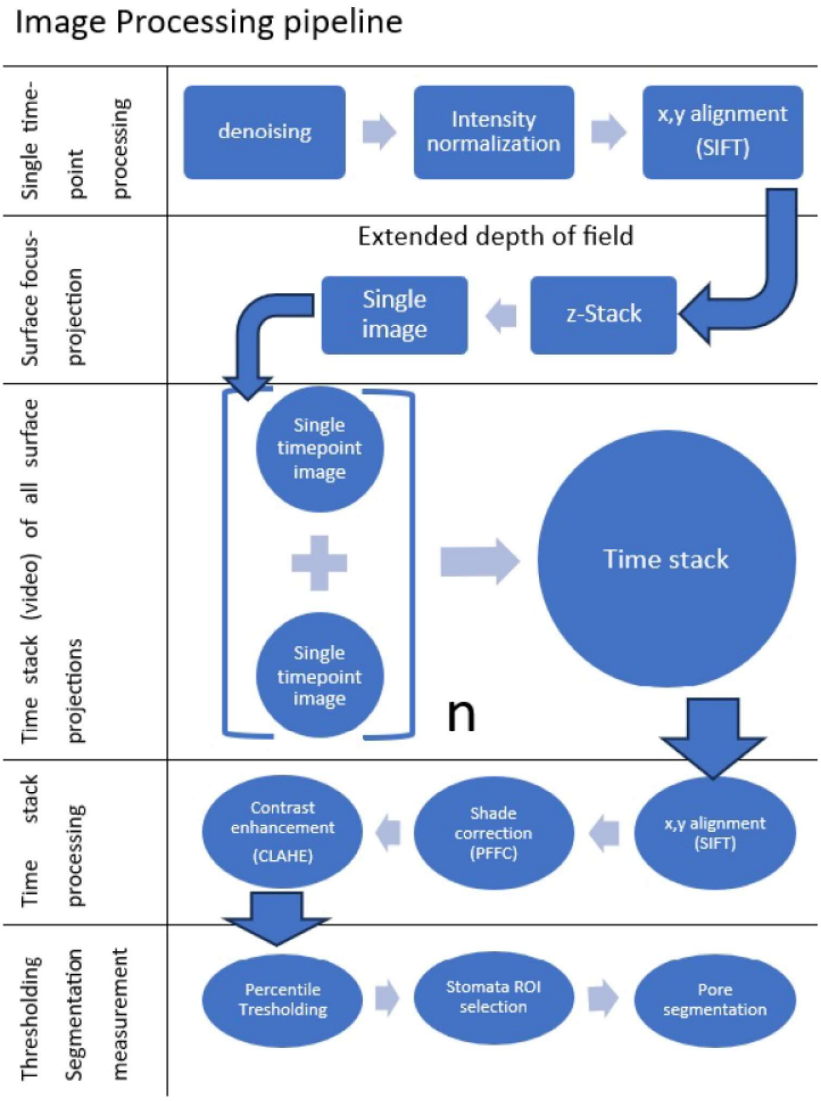

Figure 2. Flow chart of image processing pipeline. Single images belonging to an image stack were denoised and their contrast was enhanced by intensity normalization (SM-Methods-Analyses). Images with different z-axis position in a stack were then aligned to correct for minor movements of the leaf surface in x or y directions (surface parallel to the microscope's objective). The extended depth of field

plugin processed the stack to create a single focus projection of leaf surface (Fig. 3A). Each surface projection timepoint was added together in a video of the entire experiment. The images in these videos were again aligned to correct for movements in the x and y directions, shade corrected (Fig. 3B) and their contrast was enhanced (Fig. 3C). Automated thresholding of time stacks was done with Percentile (Chrysanthemum, Fig. 3D) or Berndsen mode (Maize). Stomatal positions were manually selected with the selection tool, the pore area was segmented, and quantified with the analyze particles menu.

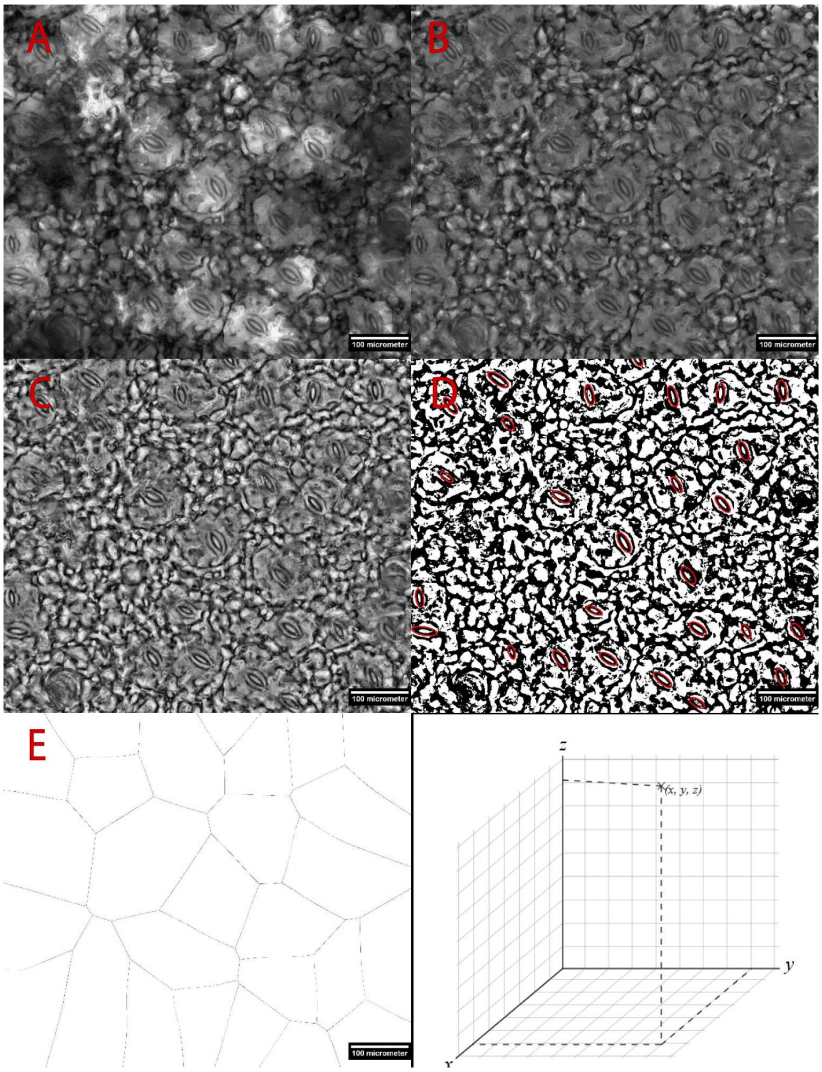

Figure 3. Example of time-stack processing with a single surface projection of Chrysanthemum. A. Surface projection output from extended depth of field (Forster *et al.*, 2004) *. B. Image in A processed with pseudo flat field correction (PFFC, (Brocher, 2015). C. Image in B processed with contrast limited adaptive histogram equalization (CLAHE, (Reza, 2004). D. Image in C after thresholding with the Percentile method (Doyle, 1962). Red ROIs are drawn manually with the elliptical selection tool. E Voronoi diagram drawn based on the elliptical selections of stomata in D, only the Voronoi that are fully resolved are quantified. The scale bar indicates 100 micrometers.*

With A(t) the stomatal aperture at time t, A_{max} the maximum aperture at the final steady-state (SS), $A_{0\text{-}i}$ the aperture at initial SS, λ the time lag of the response (min) and k the time constant (min), a measure of

265 the rapidity of the response. For stomatal closure, $A_{min\text{-}d}$ was defined
266 as the final aperture at SS with $A_{0\text{-}d}$, the aperture at the start of the
267 closing response. k and λ were separately quantified for open and
268 closing responses, using subscripts I (increase) and d (decrease),
269 respectively

270 $$A(t) = (A_{min-d} - A_{0-d})\, e^{-e^{(\frac{\lambda_d - t}{k_d} - 1)}} + A_{0-d}. \quad \text{(Eqn. 2)}$$

271 SM Fig. 1A provides an example of the fit of the kinetics for a single
272 Chrysanthemum stoma.

273 Parameters that relate to SS pore aperture, such as k or A_{max} were only
274 compared if the SS could be fitted with confidence (final aperture
275 value in high light period (1000-1500 µmol photons $m^{-2}s^{-1}$) ≥ 90% of
276 fitted value of A_{max}). In the 180-minute shade-sun-shade experiments
277 in Chrysanthemum (SM Methods Lighting and Imaging Protocols), the
278 steady state was not fitted with confidence, therefore k_i, $A_{max\text{-}i}$ and k_d
279 were ignored in the analyses.

280 Because pore apertures in maize stomata frequently oscillated, we
281 only fitted the first opening kinetics until a quasi-steady state (QSS)
282 had been reached, to fit the starting aperture ($A_{0\text{-}i}$), the opening delay
283 (λ_i) and the initial maximum opening speed (max $dAdt_i$) (SM Fig 1B).
284 The maximum aperture was not derived from fitting, but instead the
285 maximum value obtained under high light intensity was used (SM Fig
286 1B). For stomata that opened to a complete steady state, we report
287 all fit values. During closure, we again fitted only the first closing
288 kinetics, until a QSS was reached for stomata that re-opened
289 afterwards (SM Fig 1B). The minimum aperture after closing ($A_{min\text{-}d}$)
290 was taken from the fitted curves, because none of the stomata closed
291 further.

292 Maximum opening and closing speeds (max $dAdt_{,\ I}$ and $_d$) were
293 calculated by finding the maximum of the first derivative for the fitted
294 curves within the time range of the fitted data (no extrapolation).

295 Some stomata were excluded from data analysis. Reasons to exclude
296 stomata were: a) bad segmentation due to low local image quality,
297 such as when a stoma shaded by a trichome, b) incomplete stomatal
298 pore on the edge of an image, c) 'false stomata' stomata that never
299 opened while image quality was not compromised, d) low-quality fit.
300 Quality of fit was assessed by adjusted R-squared statistic of the fit
301 (ideally close to 1), the structure in the residuals (ideally random noise
302 without structure) and error estimates of the fitted parameters
303 (ideally <10%, but no larger than 100%).

304 For Chrysanthemum 2% (3/124) of closing stomata were omitted
305 from the kinetic analyses because the fit was bad (adjusted R-
306 squared<0.8).

307 For maize, 17% (5/29) of opening and 21% (6/29) of closing kinetics
308 of stomata were omitted from the kinetic analyses, as their fast
309 kinetics could not be fitted accurately (40%-900% fit error) due to the
310 measuring interval of the microscope. We report more on these
311 stomata in the results.

312 *Categorization of kinetics*

313 Chrysanthemum

314 Before a step increase in light intensity, stomata were categorized by
315 fitting a straight line through the initial time course of pore aperture
316 in low light. If the slope was not significantly different from zero, the
317 stoma was categorized as SS, if the slope was positive as opening and
318 if the slope was negative as closing. If an upward trend was followed
319 by a downward trend or vice-versa, the stoma was categorized as
320 oscillating.

321 In the sun period and the final shade period, stomata were
322 categorized as delayed if the lag (λ) in minutes was larger than 0 and
323 the lag fit error was less than 50% of the fitted value.

324 Stomata in the final shade period were categorized as closing to a QSS
325 if the final QSS fit value was reached with confidence and further data
326 trend did not fall outside fit error for the QSS value. If instead they did

327 not reach a QSS, they were categorized as closing. If further data trend
328 fell outside the fit error for the QSS value and were higher than the
329 QSS, they were categorized as closing and re-opening.

330 Maize

331 Stomata were categorized as oscillating between open and closed if
332 they fully closed and re-opened or opened and fully closed in the
333 initial growth light period (I) (e.g. in SM Fig. 1B).

334 Stomata were categorized as opening and oscillating (saturating light,
335 period II) or closing and oscillating (final growth light, period III) if after
336 initial opening/closing their apertures were stagnating and thereafter
337 opening/closing further for more than five time-points in a row.

338 *Morphological measurements*

339 Guard cell length (GCL) was measured in Fiji by manual use of the
340 straight-line tool in the image at the last timepoint of the period with
341 1000 (Chrysanthemum) or 1500 µmol photons $m^{-2}s^{-1}$ (Maize), the
342 timepoint where stomatal aperture was generally maximal. GCL was
343 taken as a proxy for stomata size because it was clear for all stomata.
344 In contrast, guard cell width and surface area suffered from the
345 unclear borders of guard and pavement cells.

346 A Voronoi plot (Fig. 3E), which connects lines with equal distance to
347 the borders of each neighbouring stoma, was created via the Voronoi
348 tool (in the Fiji software), and each surface was measured via the
349 'analyse particles' menu. Resulting data were used to test for
350 relationships between the leaf area that could be assigned to a given
351 stoma ('Voronoi area') and that stoma's aperture and kinetics. Only
352 Voronoi surface areas that were fully inside the image were
353 considered in this analysis.

354

355 Because our method depends on the automated focus projection of
356 the z-stack (the reduction into a single image that represents the
357 entire surface within the FOV), we compared it to the human

operator: manual selection of the best focus position per pore. We compared the results for ten stomata with a good distribution within the FOV for 100 stacked images per 119 time points during shade-sun-shade transition for *Chrysanthemum*. Further image processing, segmentation and quantification of the pore area were automated and following the identical protocol for both manual selection and focus projection.

Plant material and growing conditions.

Chrysanthemum

Experiments were conducted in a previously described growth chamber (Zhang *et al.*, 2024). Chrysanthemum (Deliflor Chrysanten, Maasdijk, the Netherlands) plants that had been grown in plastic pots (diameter 14 cm, filled in with potting soil) were cut back at the third or fourth node to allow for the formation of new axillary buds.

Maize

Seeds (Tasty sweet F1, Buzzy) were germinated and grown in plastic pots (diameter 14 cm, filled in with potting soil) for one week at 160 μmol m^{-2} s^{-1} followed by two weeks at 500 μmol m^{-2} s^{-1}. The photoperiod was 18:6 (light/dark) with temperature 22/20 °C (day/night). Plants were irrigated twice per day (at 9:00 and 17:00 h) with nutrient solution, using an automatic ebb and flow system. Experiments were conducted in a different room because the growth chamber had a layout with stacked layers for plant growth with too little space to fit the microscope. Temperature in the measurement room was 23°C and RH was 70%. Plants were acclimated for at least 60 min in the measurement room before measurements were started.

Stomatal aperture measurements

Stomatal apertures were measured on the youngest fully expanded leaf (Chrysanthemum) or the oldest developing leaf (Maize) in the middle between the leaf edge and the midrib. A screen was used to

shade the measured plant from direct growth chamber lighting during aperture measurements (Chrysanthemum). All lighting and imaging protocols used are reported in the SM Methods section.

Statistical tests

Normality tests for the distribution of fit or measured parameters were performed with Shapiro-Wilkins test. KWANOVA and paired Wilcoxon signed rank tests were used to test for significant differences between sets of parameters that were not normally distributed. Spearman's correlation was calculated between sets of parameters that were not normally distributed. For normally distributed data, ANOVA, students t-test and Pearson correlations were used. All statistical tests were performed in Origin (OriginLab).

Results

Our portable microscope enabled the imaging of stomatal dynamics of Chrysanthemum and Maize by its selective use of green light, with limited effects on stomatal movement (SM Fig. 2) (Jones *et al.*, 2022) for imaging at a low light intensity, while using stepwise changes in light intensity (red/blue spectrum) to trigger changes in stomatal aperture.

Comparison of stomatal pore area dynamics between automatic and manual selection of best focus per pore

The dynamics of the pore area in the focus projection images (automatic) were well correlated with those in the manually selected best single focus images (Fig. 4A, SM Fig. 3, r >97% P<0.001). However, the pore area tended to be smaller when derived automatically: pores were on average ten μm^2 smaller in automatic than in manual images (Fig. 4B). To investigate if this difference in pore area arose from spatial dependence of image quality, we correlated the difference against positional coordinates of the stomata. We found that these differences between automatic and manual-derived pore area were

neither correlated to the x (r=-0.16, not significant (NS)), y (r=0.2, NS) position of the pore in the image, nor to the distance of the pore to the image edge (ρ=0.24, NS), nor to the position in the stack of the manual images (r=-0.36, NS). Further, pore opening and closing speeds in the automatic images were similar in the manual images, as indicated by the maximum opening and closing speeds of the fitted curves (Opening: automatic 0.99±0.05, manual 0.93±0.04 $\mu m^2 min^{-1}$, Closing: automatic 2.1±0.3, manual 1.9±0.3 $\mu m^2 min^{-1}$, NS). In conclusion, the automatic method can correctly assess the kinetic parameters of the stomata but may underestimate the true pore area.

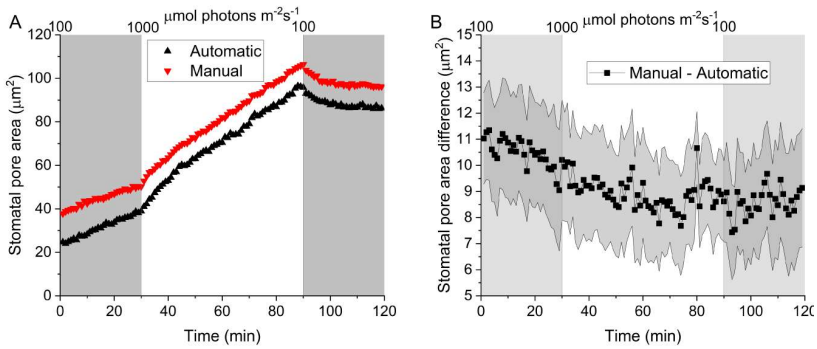

Figure 4. An Example of kinetics of one Chrysanthemum stoma analyzed with the focus projection (automatic) method or in the manually selected best single focus images (manual) demonstrating their correlation. All individual stomata curve pairs are in SM Fig 2. B Averaged difference in pore area between the same pore analyzed in the automatic images and the Manual images in all timepoints of the shade-sun-shade transition. The shaded area around the curve indicates the standard error of means (n=10). Light grey blocks indicate shade periods.

Movement of the leaf surface upon light intensity change

Because we recorded changes in the position of the leaf surface via automatic adjustments by the step motor of the microscope, we could observe the movement of the leaf surface upon changes in light intensity (Fig. 5). Specifically, after the switch from 100 to 1000 µmol m^{-2} s^{-1} for Chrysanthemum, there appeared to be some shrinkage or bending of the leaf, as its surface moved away from the camera, whereas upon the transition from 1000 to 100 µmol m^{-2} s^{-1}, the opposite happened (Fig. 5). These leaf surface movements had no impact on imaging, because the FOV of the leaf was always captured in focus within the stack. Leaf surface movements resulted in a minor

displacement of the position of the leaf surface in the stack (SM Fig. 4). Thus, the autofocus software adjusts the z-position of each new image stack based on the previous z-position, because the leaf surface shifts hundreds of micrometers when light intensity changes.

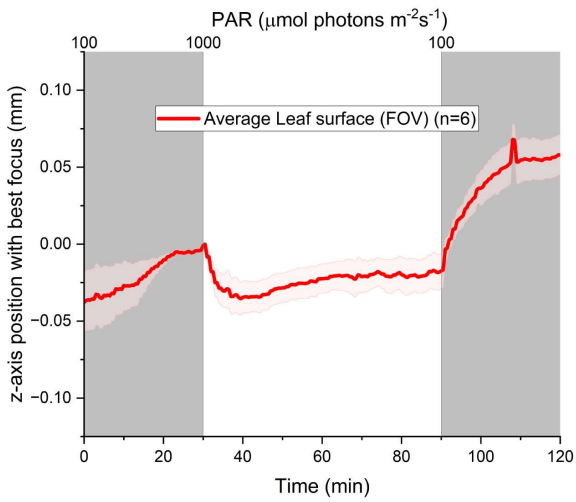

Figure 5. Position on the z-axis of the imaged area of the Chrysanthemum leaf surface where the largest area of leaf surface was in focus during the shade-sun-shade experiment. The red curve indicates the average of six biological replicates, and the shaded area indicates the standard error of the mean. The z-axis position at t=30 min was set to zero for each measurement before averaging. The focus position (y-axis) indicates the middle position of 100 images taken per minute, each of which was spaced one µm apart.

Stomatal dynamics of maize leaves during transitions between growth and saturating light intensity

A central question in research on stomatal biology is whether morphological parameters of individual stomata such as their size (GCL) and the mesophyll area for which they provide gas exchange (Voronoi area) impact their kinetics. To investigate this, we measured these morphological parameters and quantified the kinetic responses of 29 stomata (45%) of four maize plants during a transition from growth light intensity (500 µmol m^{-2} s^{-1}) to photosynthetically saturating light intensity (1500 µmol m^{-2} s^{-1}), and back to growth light intensity (in SM Fig 1). 35 (55%) stomata were unresolved of which eleven were on an image edge, 12 opened but pore area could not be segmented, one clustered smaller stoma did not open and for eleven

479 stomata the pore image quality was so poor that it could not be
480 determined if they opened or not. Nine of these stomata with very
481 poor image quality were near a vein.

482 We observed a number of different responses among the resolved
483 stomata which we then categorized as closed, open, or oscillating
484 between open and closed, under initial exposure to growth light (I),
485 opening towards a new SS, or opening and oscillating, during the
486 saturating light period (II) and closing towards a new SS, or closing and
487 oscillating, during the final period (III) (Fig. 6A). Stomata were
488 observed to have combinations of all categories of period I-III except
489 open (I) – open and oscillating (II) – closing and oscillating (III).
490 Interestingly, GCL was different between all categories in the initial
491 growth light period (I, Fig. 7A). In contrast, no differences were found
492 between kinetic categories in periods II-III for GCL and in periods I-III
493 for Voronoi area (SM Fig 5 A-E). For these stomata, their initial state
494 in the growth light was thus strongly linked to their GCL, but the
495 occurrence of oscillations in their subsequent kinetics was not.

496 The starting aperture and the maximum aperture during the
497 saturating light period (II) were different between stomata that were
498 closed or oscillating and those that were open during the initial period
499 with the growth light (I) (Fig 7BC). In contrast, the lag time before the
500 opening response under saturating light (II) was smaller for initially
501 open or oscillating stomata than for initially closed stomata (Fig 7D).
502 Thus, while both closed and oscillating stomata initially had a low and
503 similar aperture, the oscillating stomata were equally fast responding
504 as the open stomata from the initial period, while the closed stomata
505 were not. No differences were found in aperture or opening lag in
506 saturating light between stomata that were opening with or without
507 oscillations in saturating light (SM Fig 5 F-G).

508 For period III (1500->500 µmol photons m^2s^{-1}), the apertures after the
509 initial closing response were again minimal for closed and largest for
510 stomata that were categorized as open in period I (Fig 7E). Stomata
511 that were opening or closing with oscillations were not different in

aperture after the initial closing than those without oscillations (SM Fig 5 I-K).

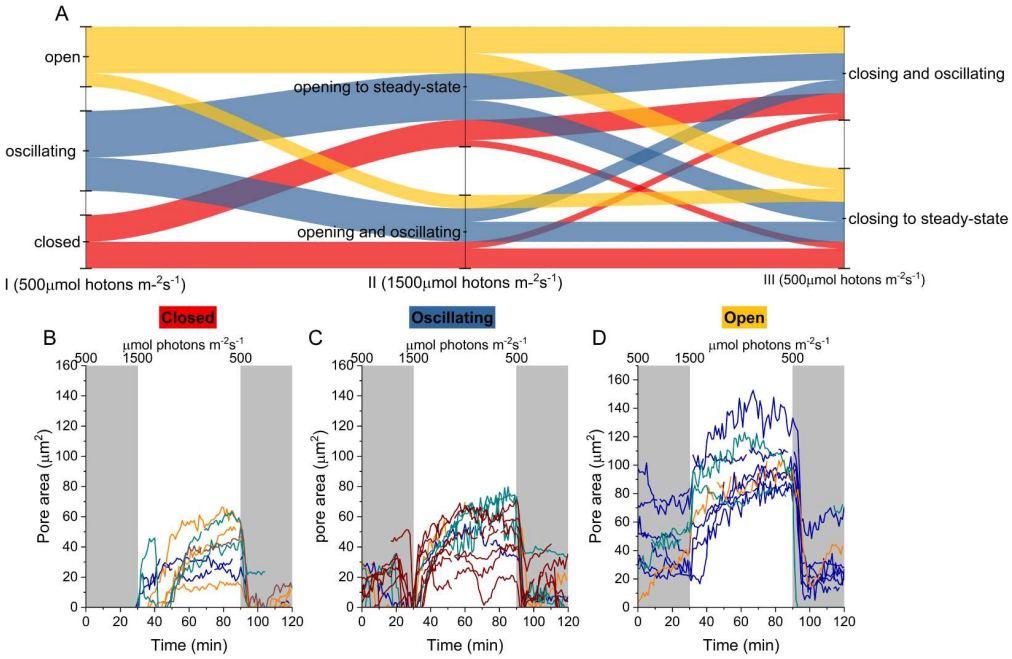

Figure 6 Categorized kinetics of 29 maize stomata during transitions from growth light to saturating light and back to growth light intensity. ***A.*** *Categorized kinetics during the three periods (I) initial growth light 500 µmol photons $m^{-2}s^{-1}$ (30 min), (II) saturating light 1500 µmol photons $m^{-2}s^{-1}$ (60 min) and (III) return to growth light intensity 500 µmol photons $m^{-2}s^{-1}$ (30 min). The thickness of bands in A indicates the fraction of stomata in that category. Colored curves in A indicate how the fraction of stomata within the starting period categories transition to the categories in period II and III. Kinetics in period I were categorized per stoma as being* ***B*** *closed,* ***C*** *oscillating between open and closed or* ***D*** *open. Stomata categories during the saturating light period were opening towards SS or opening and oscillating. Similarly stomatal categories during period III were closing towards SS, or opening and oscillating. Colors of curves in B-D indicate individual plants.*

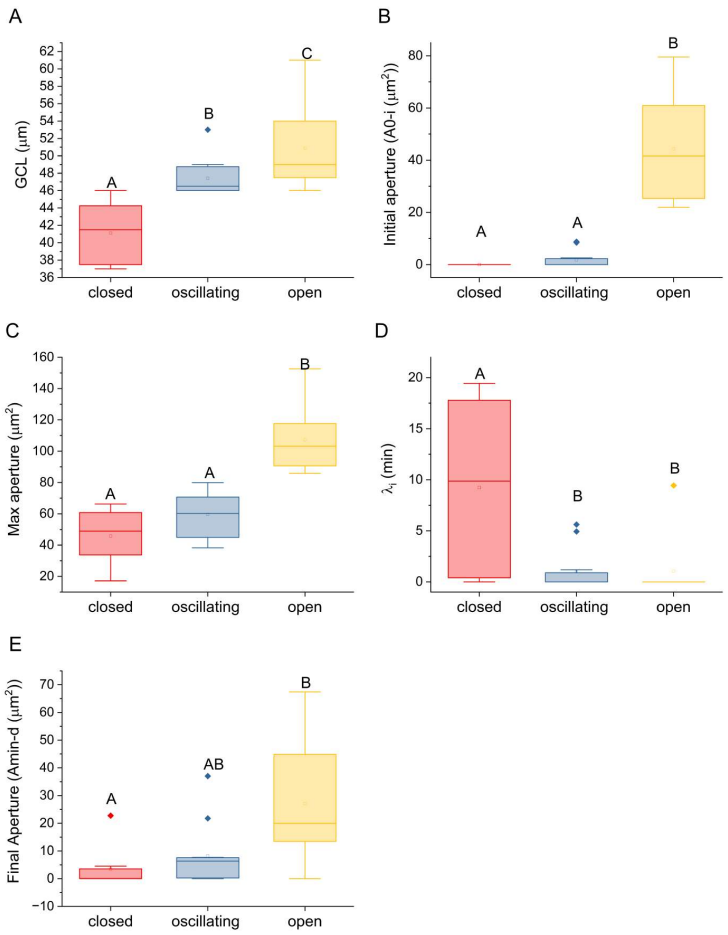

Fig 7. Categories of maize stomatal behavior under growth light intensity, and relationships with morphology and kinetics during light-driven opening and closing of maize stomata. ***A*** *Guard cell length* ***(****GCL).* ***B*** *Initial pore aperture,* ***C*** *maximum pore aperture and* ***D*** *lag time (λ_i) until opening response in the saturating light period (II).* ***E*** *pore aperture after initial closing in the final period (III). Significant differences between kinetic categories by ANOVA (A, C) or KWANOVA are indicated by different capital letters (P<0.05). Squares represent the average and lines the median (Q2. Box outlines represent the lower (Q1) and upper quartile (Q3), and the whiskers indicate Q0 and Q4.*

Speed of stomatal movement

Maximum opening speed in period II and closing speed in period III were not different between any of the stomata in the categories of periods I-III (SM Fig 6 A-F) and are therefore presented for all stomata in Fig 8A. Unlike the maximum opening speed, the maximum closing speed was positively correlated to guard cell length (ρ=0.51, p=0.01). The average maximum closing speed was seven times larger than the average maximum opening speed, and maximum opening and closing speeds were positively correlated (ρ=0.47, p=0.03). Similarly, the time

constant of stomatal opening, k_i, was eight times larger than the time constant for stomatal closure, k_d (Fig. 8B). Average maximum opening and closing speeds were underestimated, because the fastest stomata (five opening and six closing) were excluded from the speed analyses, as their speed could not be fitted correctly. These stomata opened or closed to a SS within one time point with a large difference in aperture (e.g. k_i <0.5 min). To eliminate that these fast responses were not processing errors, we again compared the automatic processing to the manually selected best focus per pore. The images of the time-points at the transition as well as the kinetics (e.g. in SM Fig. 7) validate the absence of processing artefacts. These stomatal responses are thus truly speedy outliers.

In conclusion, the annotation of the considerable variation in the kinetics of individual stomata demonstrates the ability of our method to identify and quantify relations between morphological parameters such as guard cell length and kinetics for individual stomata.

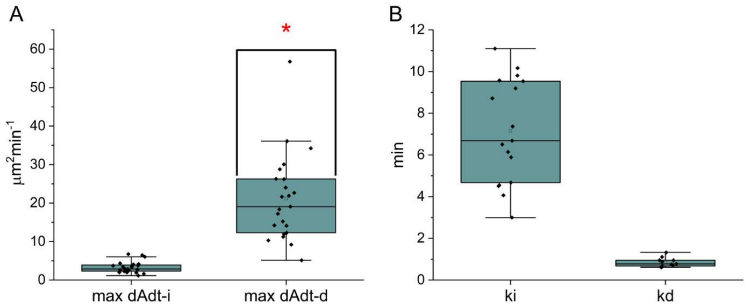

Fig. 8. Parameters characterizing rates of stomatal opening and closure in maize stomata during transitions from 500 to 1500 back to 500 µmol photons m^2s^{-1}. ***A*** *maximum opening and maximum closing speeds (n=23). Asterix indicates significant correlation with GCL (ρ=0.51, p=0.01).* ***B*** *k_i, opening time constant for stomata that opened to SS (n= 17). k_d, closing time constant for stomata that closed to SS (n= 11). Squares represent the average and lines the median (Q2. Box outlines represent the lower (Q1) and upper quartile (Q3), and the whiskers indicate Q0 and Q4.*

Stomatal dynamics of *Chrysanthemum* leaves during a shade-sun-shade transition.

To further demonstrate the power of our method, we tested it in a shade-sun-shade transition on leaves of Chrysanthemum, where photosynthesis typically reaches a SS during the sun phase (60 min),

but stomatal aperture does not (SM Fig 2 (Zhang *et al.*, 2022, 2024)). The rate of stomatal opening at 60 min of high light is higher and in absolute terms more variable than close to SS pore area at 180 min for individual stomata (SM Fig. 8, (t=60 min) 1.25 ± 0.09 > (t=180 min) 0.25 ± 0.05 $\mu m^2 min^{-1}$). Therefore, we investigated the effect of the change in irradiance on individual stomata, when individual apertures and rates of opening were more heterogeneous than at steady state, to derive relations to subsequent responses during the shade phase. We imaged the leaves of six plants split over two cultivation periods. After image processing, 124 opening and 95 closing kinetics out of 158 stomata in the FOV were resolved (Fig. 9).

While average stomatal aperture was in a SS in the initial shade condition (Figure 9, 0-30 min), some individual stomata showed minor movements by either slightly opening or slightly closing. 47 stomata were closed, 25 were open in a SS, 27 were opening, 21 were closing and one stoma was open but oscillating. Closed stomata had smaller GCL than those that were closing in initial shade (Fig. 10A). In addition, closed stomata also had smaller Voronoi area than those that were closing or in a SS in initial shade (Fig. 10B). Apertures at the start of the sun period were not different between opening, SS, closing or oscillating stomata in the initial shade (SM Fig. 9A).

After the light intensity was increased, 70% of resolved stomata (87) immediately opened their pores towards a SS, while the rest showed a lag in their response of up to 40 min (Fig. 9). Most stomata with an opening lag were closed in the initial shade (SM Fig 9B). Maximum opening speeds between stomata with and without delayed opening were not different (SM Fig 9C). Maximum aperture in the sun phase was lower for initially closed stomata than for opening, closing or SS stomata in the initial shade (SM Fig. 9D). Similarly, stomata with a delayed opening response reached a lower maximum aperture during the sun phase (SM Fig 9E).

The light intensity decrease led to an immediate closing response of 32 stomata (33%), of which 18 reached a quasi-steady-state (QSS),

610 four closed and re-opened and ten did not reach a QSS (all ten were
611 on the same leaf). We use QSS here, because the average final shade
612 aperture was larger than the average initial shade aperture (A_{min-d}
613 23±3 μm^2 > A_{0-i} 13±2 μm^2, mean+SE, paired sample Wilcoxon Signed
614 Ranks Test, $P<0.005$), and because further closing could have occurred
615 after 30 min in the final shade. Immediately closing stomata that did
616 not reach a QSS had a larger aperture at the time of the light intensity
617 decrease than those that reached a QSS (Fig 10C).

618 53 stomata (54%) had a delayed closing response, of which 38
619 reached a QSS with no differences in aperture at the time of the light
620 intensity decrease between these two groups (Fig. 10C). No
621 indication was found that delayed stomata could compensate for their
622 delay by a faster closure, because the maximum closing speed was
623 similar between delayed and immediately closing stomata (Fig. 10D).
624 19 stomata (19%) did not close at all within the 30 min sun-shade
625 transition. These stomata were not evenly distributed among the
626 biological replicates (numbers per replicate: 15:1:3:0:0:0) and had a
627 similar aperture at the time of the light intensity decrease than the

stomata in the other closing categories (74 ± 5 μm^2).

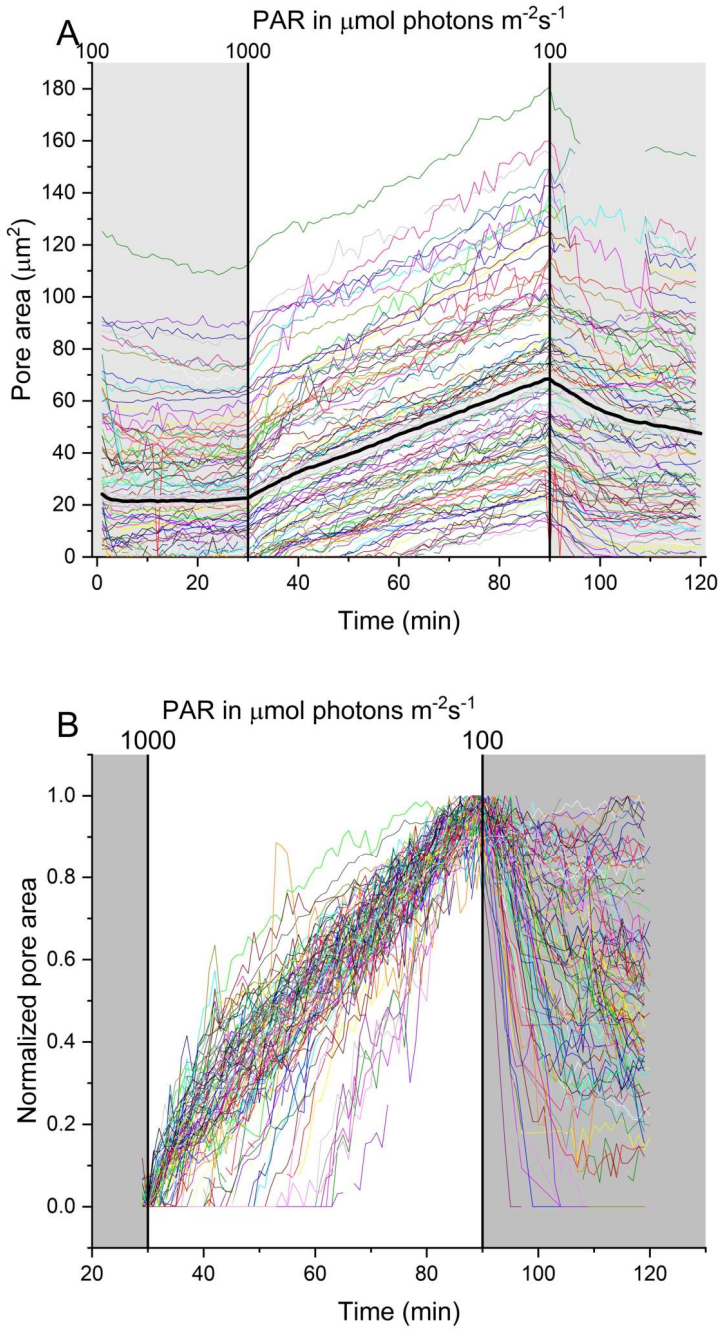

Figure 9. Stomatal pore area changes upon a shade-sun-shade transition. Single lines show values of 124 individual stomatal pores from six chrysanthemum plants. The thick black curve represents the average, and the grey area the standard error of the mean. During the second shade period, a temporary loss of focus during one measurement caused fewer data points to be recorded. B Kinetics of all stomata shown in A, normalized to 0 at t=29 min just before the light intensity was increased and to 1 for the maximum aperture reached at 1000 µmol photons $m^{-2}s^{-1}$, highlighting the differences in opening lag (λ_i) and stomatal closure.

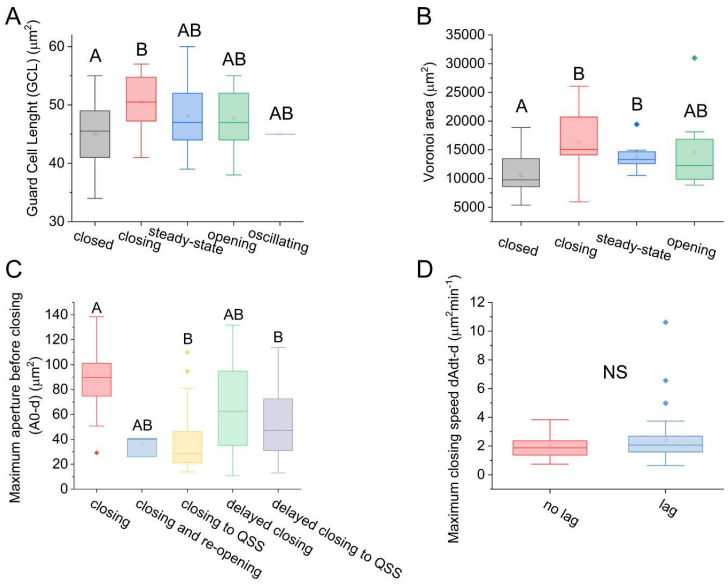

Fig. 10 Morphological and kinetic parameters of categorized Chrysanthemum stomata during a shade-sun-shade transition. ***A*** *Guard Cell length (GCL) and* ***B*** *Voronoi area compared between the kinetic categories of the initial shade phase. Number of stomata per category: 47 closed, 25 open in a steady-state, 27 opening, 21 closing and one stoma was open but oscillating. Voronoi area could only be quantified for 27 closed, 12 open in a steady-state, ten opening and 9 closing stomata* ***C*** *Maximum pore aperture in the sun phase before closing. Number of stomata per category: 12 closing, three closing and reopening, 16 closing to QSS, 15 delayed closing and 38 stomata in delayed closing to QSS.* ***D*** *Maximum pore closing speed compared between categories with and without closing lag (λ_d) of the final shade phase. Squares represent the average and lines the median (Q2. Box outlines represent the lower (Q1) and upper quartile (Q3), and the whiskers indicate Q0 and Q4.*

Of all parameters, only guard cell length was normally distributed (Shapiro Wilkins test, $p<0.001$), therefore Spearman's nonparametric ρ was used to investigate correlations. A larger aperture during the first shade phase ($A_{0\text{-}i}$) was strongly correlated with a larger maximum aperture in the sun phase $A_{0\text{-}d}$, and moderately correlated to the QSS aperture during the second shade phase $A_{min\text{-}d}$ (Fig. 11). $A_{0\text{-}d}$ was also moderately correlated to the maximum opening speed, $dAdt_I$ (Fig. 11). The time lag of the opening response (λ_i) was negatively correlated to $A_{0\text{-}I}$, GCL, Voronoi, $A_{0\text{-}d}$, $A_{min\text{-}d}$, λ_d, and positively to the maximum closing speed, $dAdt_d$ (Fig. 11). Interestingly, the time lag of the closing response (λ_d) was correlated to $A_{0\text{-}i}$ and $A_{0\text{-}d}$ (Fig. 11).

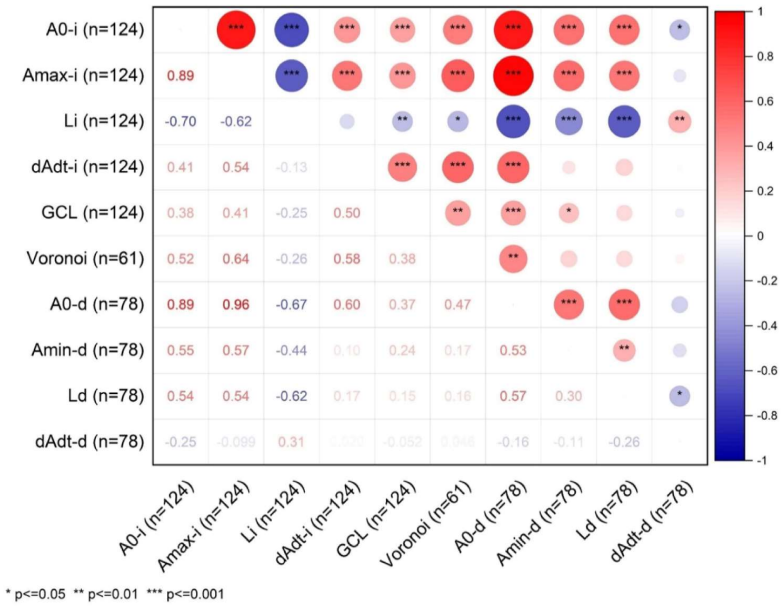

Figure 11. Spearman's correlation matrix between parameters of individual Chrysanthemum stomata (based on Fig. 9). A_0, fitted steady-state aperture under 100 µmol photons $m^{-2}s^{-1}$ PPFD. A_{max}, maximum aperture under 1000 µmol photons $m^{-2}s^{-1}$ PPFD; Li/Ld, lag (λ_i/ λ_d) in the response time of stomatal aperture to a step increase or decrease in PPFD; dAdt, maximum rate of stomatal opening (-i) or closing (-d) to an increase or decrease in PPFD from 100 to 1000 µmol photons $m^{-2}s^{-1}$ or vice versa. Anatomical parameters of guard cell length (GCL) and Voronoi area were also compared. The Voronoi area represents the fraction of the leaf surface that is within the shortest distance to that stoma. $A_{0\text{-}d}$, fitted final aperture under 1000 µmol photons $m^{-2}s^{-1}$, $A_{min\text{-}d}$, predicted final steady-state aperture under 100 µmol photons $m^{-2}s^{-1}$ (QSS).

Among the anatomical parameters, Guard cell length (GCL) was moderately correlated to the maximum opening speed $dAdt_{max\text{-}i}$, initial $A_{0\text{-}I}$, maximum $A_{0\text{-}d}$, and final aperture $A_{min\text{-}d}$, as well as the Voronoi area (Fig. 11). Additionally, the Voronoi area was moderately correlated with $A_{0\text{-}i}$, $A_{min\text{-}d}$ and the maximum opening speed $dAdt_{max\text{-}i}$, (Fig. 11).

In conclusion, our method resolved ten different kinetic and non-kinetic parameters for up to 78% of the *Chrysanthemum* stomata within the FOV to generate new insights into the WUE of individual stomata.

Discussion

We have presented a real-time *in planta* microscope, which provides a new way to study the opening and closure of individual stomata in the growth environment. This method facilitates analyses of

689 individual stomatal dynamics in relation to their local morphology
690 (Voronoi) and anatomy (Guard Cell Length). Our hardware and
691 method are distinct from the few previous studies that have imaged
692 stomata *in planta* (Kaiser and Kappen, 1997, 2001; Kaiser, 2009;
693 Grantz, Zinsmeister and Burkhardt, 2018). The main differences to
694 previous approaches, as well as their advantages and disadvantages,
695 are listed in Table 1.

696 *Table 1 Differences between this work and prior studies (Kaiser and Kappen, 1997,*
697 *2001; Kaiser, 2009; Grantz, Zinsmeister and Burkhardt, 2018) with their advantages*
698 *and disadvantages*

Difference	**Advantage**	**Disadvantage**	**Study**
525 nm versus 880 nm imaging light	Higher optical resolution	Imaging light is photosynthetically active, closing effect on stomata	(Kaiser & Kappen, 1997, 2001)
Autofocus per stack instead of per pore	Imaging speed is not limited by number of stomata, but by stack size	Can cover stomata in only a small area of the leaf (~1 mm^2)	(Kaiser & Kappen, 1997, 2001; Kaiser, 2009; Grantz et al., 2018)
Kinetic model fitting	Quantitative comparison of fit parameters	-	
No Gas exchange chamber	Boundary layer thickness is close to natural	No information on leaf bulk gas exchange	(Kaiser & Kappen, 1997, 2001; Kaiser, 2009; Grantz et al., 2018

699

700 A major contrast with prior studies is that the way the leaf is clamped
701 was minimally invasive to the microenvironment of the leaf, with free
702 transpiration on both sides of the leaf, because no gas exchange
703 measurements were performed. Unlike in gas exchange cuvettes that

use fans to stir the air and thus minimize boundary layer thickness, in our method the thickness of boundary layer was not regulated, reflecting the natural state of the leaf. Another major difference was the sampling of stomata: prior studies have randomly sampled stomata over a large area (>1 cm^2), whereas we resolved as many stomatal kinetics as possible within ~1 mm^2, to relate their kinetic behavior to the local morphology on the surface of the leaf (e.g. Voronoi area). We reached a higher time resolution of, on average, 21 stomata min^{-1} for *Chrysanthemum*, but seven stomata min^{-1} for maize, compared to 75 stomata once every 6-7 min in *Vicia Faba* (Grantz, Zinsmeister and Burkhardt, 2018). Sampling in ~1 mm^2 means however that variations in dynamics over greater distances are missed. Another major difference to previous studies is that we fit a kinetic model to individual stomatal aperture kinetics, to be able to quantitatively compare them and derive functional relationships. Further, our method detects changes in leaf thickness or bending under dynamically changing light intensity (Fig. 5), a feature that may enable it to be used in studies investigating functional relationships between leaf morphology, leaf water relations, and stomatal pore area (including dynamic changes in all of these properties).

Our method measured smaller pore area compared to manual selection of the best focused single image per pore (Fig. 3). The smallest part of the pore may, however, not necessarily be entirely in focus in a single image, especially for large stomata. It could therefore be plausible that the true pore area lies between both types of measurements of pore area. Implementation of the state-of-the art in computer vision solutions, such as StomaAI (Sai *et al.*, 2023), for stomatal measurements and segmentation may increase the resolving power.

Comparing Maize and Chrysanthemum

In contrast to Chrysanthemum, where 78% of stomata were clearly resolved, a significant portion of stomata in maize (55%) remained unresolved. This discrepancy was partly due to the more transparent

737 leaf surface in maize, which allowed structures beneath the surface
738 to be visible. As a result, the surface projection algorithm faced
739 challenges, producing lower-quality images compared to those of
740 Chrysanthemum, where this issue did not arise.

741 The GCL for Maize and Chrysanthemum was on average 47 µm (Fig. 7
742 A, Fig. 10A), with either dumbbell (Maize) or elliptic
743 (Chrysanthemum) anatomy. Although their length was similar, the
744 kinetics were much faster in Maize stomata compared to
745 Chrysanthemum, with higher opening and closing speeds and less lag
746 (Fig. 9, SM Fig 8 C, D), related to their anatomy (Lawson and Vialet-
747 Chabrand, 2019). In addition, the different light intensity changes and
748 the different leaf age and developmental stages may have affected the
749 relative difference in kinetics.

750 Stomatal size was found to be negatively correlated with WUE across
751 different Arabidopsis ecotypes (Dittberner *et al.*, 2018). A high WUE
752 is typically associated with a fast rate of stomatal closure (Lawson and
753 Vialet-Chabrand, 2019), and smaller stomata have indeed often been
754 observed to open or close faster than larger stomata (Drake, Froend
755 and Franks, 2013; Kardiman and Ræbild, 2018; Durand *et al.*, 2019).
756 In contrast, we found a strong positive correlation between GCL and
757 maximum opening speed for Chrysanthemum as observed before for
758 elliptical/kidney-shaped stomata (McAusland *et al.*, 2016), as well as
759 a positive correlation between GCL and maximum closing speed for
760 Maize. Maximum opening and closing speeds of individual stomata
761 were correlated in Maize ($r=0.48$, $P<0.05$) but not in Chrysanthemum
762 (Fig. 11). The relation between stomatal size and speed may thus be
763 more complex than previously assumed. This relation could be
764 species dependent, as no correlation between stomatal size and
765 speed was found in a diverse range of plants with differing stomatal
766 morphologies and physiological behaviors (Haworth *et al.*, 2018).
767 Additionally, it may depend on the type of stimulus, since e.g. step
768 changes in light intensity and in VPD often trigger different dynamics
769 (Durand *et al.*, 2019).

Average Voronoi area was smaller for Chrysanthemum stomata (13000 μm^2, Fig. 10B) compared to Maize stomata (28000 μm^2, SM Fig. 5D). Similarly, stomatal density was higher in Chrysanthemum images (72 mm^{-2}) than in Maize (32 mm^{-2}).

Could stomatal pore oscillations in low light be a means to increase the response speed of stomata to a high light stimulus?

Maize stomata that oscillated between open and closed state in low light intensity and were closed before the light intensity changed responded faster to a high light intensity than stomata that were initially closed in a steady-state (Fig. 7 B, D). The faster opening could have benefits for carbon assimilation (Lawson and Blatt, 2014; Lawson and Vialet-Chabrand, 2019). Oscillations originate from the gain in feedback regulation (Kaiser and Paoletti, 2014; Peak, 2023); they are the result of an interaction of hydraulic effects and active osmotic adjustment of guard and epidermal cells. Oscillations have been argued to allow for a faster response to environmental fluctuations (Kaiser and Paoletti, 2014), and our data seems to confirm this for a response to high light (Fig. 7). It would be interesting to explore this phenomenon further, e.g. by using larger numbers of stomata and stimuli.

Closing lag and partial closing affect water loss of Chrysanthemum stomata under dynamic light intensity

The analysis of dozens of *Chrysanthemum* stomata produced several insights of stomatal behavior, with important repercussions for WUE: removing the average closing delay of 4.4 min would lead to 13.5% water saving during that 30 min period per average stoma, with a delayed closing response (Fig. 12). Moreover, removal of the partial closing to a QSS would save ~20%, and in combination with removal of the closing lag it would save ~40%, assuming that the maximum speed was kept the same (Fig. 12b). The extent of water saving depends on QSS relative to SS in the shade, and on the closing speed. Considering that delayed closing (51%) and partial closing to a QSS (52%) occurred frequently, it would be interesting to find out if these

targets could really be used to improve WUE (in Chrysanthemum and elsewhere). Moreover, larger aperture in high light intensity (A_{max-i}) correlated positively with the time lag for the closing response (λ_d), further enhancing the consequence for WUE. Finally, closing delays were longer for Chrysanthemum stomata that were close to the SS pore aperture at 1000 µmol photons $m^{-2}s^{-1}$ (SM Fig. 8) than for those that were not (Fig. 9) (λ_d (180 min 'Sun') 14±1 >> (60 min 'Sun') 4.4±0.4 min, P<0.0001, KWANOVA) with much larger apertures ((180 min 'Sun') 202±7 >> (60 min 'Sun') 56±4 μm^2, P<0.0001, KWANOVA) and therefore a relatively larger effect of closing delay on WUE at the SS in the 'Sun'. The larger closing delay for stomata near SS than far from SS at 1000 µmol photons $m^{-2}s^{-1}$ indicates that the closing delays were not merely related to hysteresis, e.g. switching from a fast rate of opening to fast rate of closing, but to the absolute stomatal aperture.

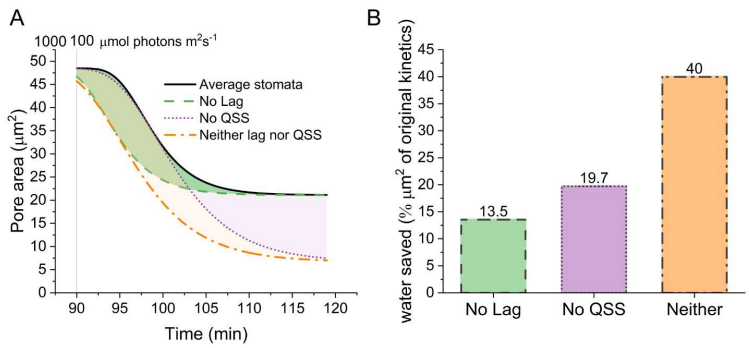

Fig. 12 Simulated impact of closing lag and partial closing of average Chrysanthemum stomata on water loss. ***A*** *Modeled closing response with Eqn. 2 of the average stomata with delayed partial closing to the QSS. Average values were taken for maximum aperture in high light, average QSS, average time-constant for partial closing (k_d) and the average closing lag λ_d. λ_d was set to 0 for no lag without changing other parameters. For no QSS, QSS was changed to the average SS (the initial average aperture in low light) and the average time-constant was adjusted to maintain the same maximum closing speed. For neither lag nor QSS, parameter changes made for no lag and no QSS were performed simultaneously.* ***B*** *Color coded areas between the curves in A normalized to the area below the average curve indicate the water saved compared to the average stomata*

Across a number of species, Deans *et al* (Deans *et al.*, 2019) found that a large stomatal conductance at high light intensity was correlated with fast closing response, to compensate in water-use efficiency. We could not corroborate this for the aperture before closing (A_{0-d}) and their maximum rate of closing (max $dAdt_{-d}$ in

individual Chrysanthemum stomata (Fig. 11), but we could for Maize (r=0.44, P=0.03). Chrysanthemum stomata with a large aperture thus have a disproportionately large negative contribution on WUE normalized for their apertures, due to the observed correlation between the aperture before closure ($A_{0\text{-}d}$) and the time lag for the closing response (λ_i), combined with a similar closing speed as stomata with a smaller aperture (Fig. 10D).

Conclusions

We showed here that *in planta* microscopy of stomata could be used to generate stomatal opening and closure dynamics of dozens of neighboring individual stomata. Our method, which uses green light for imaging and generates focus projections of the entire leaf surface within the FOV, resolved the kinetics of 78% of *Chrysanthemum* and 45% of Maize stomata, on average 21 and 7 stomata min^{-1} during light intensity transitions. We detected bending of the leaf and/or changes in leaf thickness, likely related to leaf turgor. Pore area kinetics were fitted with a model developed for stomatal conductance time courses and show the substantial variation between individual stomata. Oscillations of maize stomata were found to contribute to their faster response upon light intensity change. Chrysanthemum pores with larger apertures contributed disproportionately to a lower WUE due to their larger lag before closing than for stomata with smaller apertures. Closing lag and partial closure in Chrysanthemum even contributed on average to a 40% higher aperture area in the first 30 minutes of closure than without these features, wasting considerable water.

Acknowledgements

We thank Seven-steps-to-heaven for their in-kind support of the actinic light source. We acknowledge 4TU HTSF Plantenna for financial support. Silvere Vialet-Chabrand and Ep Heuvelink are acknowledged for helpful discussion of the results.

Competing interests

None declared.

Author contributions

Conceptualization T.B. and J. S., Hardware T.B. R.S. Software T.B., R.S., Growing facilities E.K., Experimentation T.B., Data Analyses T.B., Writing the first draft T.B., Critical review of the manuscript T.B., E.K., J.S., Funding J.S.

Data availability

All data is available on request. For more information and software updates: GitHub - Plantenna/Stomata-microscope: Non-invasive microscopic imaging of individual stomatal kinetics in the growth environment with high resolution

References

Anderson, R., Bayer, P.E. and Edwards, D. (2020) 'Climate change and the need for agricultural adaptation', *Current Opinion in Plant Biology*, 56, pp. 197–202. Available at: https://doi.org/10.1016/j.pbi.2019.12.006.

Bertolino, L.T., Caine, R.S. and Gray, J.E. (2019) 'Impact of stomatal density and morphology on water-use efficiency in a changing world', *Frontiers in Plant Science*, 10(March). Available at: https://doi.org/10.3389/fpls.2019.00225.

Blatt, M.R. (1987) *Electrical characteristics of stomatal guard cells: The ionic basis of the membrane potential and the consequence of potassium chloride leakage from microelectrodes*, *Planta*. Springer-Verlag.

Brocher, J. (2015) 'The BioVoxxel image processing and analysis toolbox', in *European BioImage Analysis Symposium*.

Buckley, T.N. (2019) 'How do stomata respond to water status?', *New Phytologist*, pp. 0–1. Available at: https://doi.org/10.1111/nph.15899.

Busch, F.A. *et al.* (2024) 'A guide to photosynthetic gas exchange measurements: Fundamental principles, best practice and potential pitfalls', *Plant Cell and Environment* [Preprint], (September 2022). Available at: https://doi.org/10.1111/pce.14815.

Deans, R.M. *et al.* (2019) 'Plant water-use strategy mediates stomatal effects on the light induction of photosynthesis', *New Phytologist*, 222(1), pp. 382–395. Available at: https://doi.org/10.1111/nph.15572.

Dittberner, H. *et al.* (2018) 'Natural variation in stomata size contributes to the local adaptation of water-use efficiency in Arabidopsis thaliana', *Molecular Ecology*, 27(20), pp. 4052–4065. Available at: https://doi.org/10.1111/mec.14838.

Dore, M.H.I. (2005) 'Climate change and changes in global precipitation patterns: What do we know?', *Environment International*, 31(8), pp. 1167–1181. Available at: https://doi.org/10.1016/j.envint.2005.03.004.

Doyle, W. (1962) 'Operations useful for similarity-invariant pattern recognition', *Journal of the ACM (JACM)*, 9(2), pp. 259–267.

Drake, P.L., Froend, R.H. and Franks, P.J. (2013) 'Smaller, faster stomata: Scaling of stomatal size, rate of response, and stomatal conductance', *Journal of Experimental Botany*, 64(2), pp. 495–505. Available at: https://doi.org/10.1093/jxb/ers347.

Durand, M. *et al.* (2019) 'Altered stomatal dynamics induced by changes in irradiance and vapour-pressure deficit under drought: impacts on the whole-plant transpiration efficiency of poplar genotypes', *New Phytologist*, 222(4), pp. 1789–1802. Available at: https://doi.org/10.1111/nph.15710.

Duursma, R.A. *et al.* (2019) 'On the minimum leaf conductance: its role in models of plant water use, and ecological and environmental controls', *New Phytologist*, 221(2), pp. 693–705. Available at: https://doi.org/10.1111/nph.15395.

Fanourakis, D. *et al.* (2021) 'Partitioning of transpiration to cut flower organs and its mediating role on vase life response to dry handling: A case study in chrysanthemum', *Postharvest Biology and Technology*, 181(July), p. 111636. Available at: https://doi.org/10.1016/j.postharvbio.2021.111636.

Forster, B. *et al.* (2004) 'Complex wavelets for extended depth-of-field: A new method for the fusion of multichannel microscopy images', *Microscopy Research and Technique*, 65(1–2), pp. 33–42. Available at: https://doi.org/10.1002/jemt.20092.

Goldstein, G. *et al.* (1995) *Environmental and physiological regulation of transpiration in tropical forest gap species: the influence of boundary layer and hydraulic properties*, *Oecologia*.

Grantz, D.A., Zinsmeister, D. and Burkhardt, J. (2018) 'Ambient aerosol increases minimum leaf conductance and alters the aperture–flux relationship as stomata respond to vapor pressure deficit (VPD)', *New Phytologist*, 219(1), pp. 275–286. Available at: https://doi.org/10.1111/nph.15102.

Haworth, M. *et al.* (2018) 'Allocation of the epidermis to stomata relates to stomatal physiological control: Stomatal factors involved in

the evolutionary diversification of the angiosperms and development of amphistomaty', *Environmental and Experimental Botany*, 151(April), pp. 55–63. Available at: https://doi.org/10.1016/j.envexpbot.2018.04.010.

Haworth, M. *et al.* (2021) 'Integrating stomatal physiology and morphology: evolution of stomatal control and development of future crops', *Oecologia*, 197(4), pp. 867–883. Available at: https://doi.org/10.1007/s00442-021-04857-3.

Horaruang, W. *et al.* (2022) 'Engineering a K+ channel "sensory antenna" enhances stomatal kinetics, water use efficiency and photosynthesis', *Nature Plants*, 8(11), pp. 1262–1274. Available at: https://doi.org/10.1038/s41477-022-01255-2.

Jones, J.J. *et al.* (2022) 'The green light gap: a window of opportunity for optogenetic control of stomatal movement', *New Phytologist*, 236(4), pp. 1237–1244. Available at: https://doi.org/10.1111/nph.18451.

Kaiser, E., Morales, A. and Harbinson, J. (2018) 'Fluctuating light takes crop photosynthesis on a rollercoaster ride', *Plant Physiology*, 176(2), pp. 977–989. Available at: https://doi.org/10.1104/pp.17.01250.

Kaiser, H. (2009) 'The relation between stomatal aperture and gas exchange under consideration of pore geometry and diffusional resistance in the mesophyll', *Plant, Cell and Environment*, 32(8), pp. 1091–1098. Available at: https://doi.org/10.1111/j.1365-3040.2009.01990.x.

Kaiser, H. and Kappen, L. (1997) 'In situ observations of stomatal movements in different light-dark regimes: The influence of endogenous rhythmicity and long-term adjustments', *Journal of Experimental Botany*, 48(313), pp. 1583–1589. Available at: https://doi.org/10.1093/jxb/48.8.1583.

Kaiser, H. and Kappen, L. (2000) 'In situ observation of stomatal movements and gas exchange of Aegopodium podagraria L. in the understorey', *Journal of Experimental Botany*, 51(351), pp. 1741–1749. Available at: https://doi.org/10.1093/jexbot/51.351.1741.

Kaiser, H. and Kappen, L. (2001) 'Stomatal oscillations at small apertures: Indications for a fundamental insufficiency of stomatal feedback-control inherent in the stomatal turgor mechanism', *Journal of Experimental Botany*, 52(359), pp. 1303–1313. Available at: https://doi.org/10.1093/jxb/52.359.1303.

Kaiser, H. and Paoletti, E. (2014) 'Dynamic stomatal changes', in M. Tausz and N. Grulke (eds) *Plant Ecophysiology: Trees in a Changing Environment*. Ecophysiol. Springer Science+Business, pp. 61–82. Available at: https://doi.org/10.1007/978-94-017-9100-7_4.

Kardiman, R. and Ræbild, A. (2018) ‘Relationship between stomatal density, size and speed of opening in Sumatran rainforest species’, *Tree Physiology*, 38(5), pp. 696–705. Available at: https://doi.org/10.1093/treephys/tpx149.

Lawson, T. and Blatt, M.R. (2014) ‘Stomatal size, speed, and responsiveness impact on photosynthesis and water use efficiency’, *Plant Physiology*, 164(4), pp. 1556–1570. Available at: https://doi.org/10.1104/pp.114.237107.

Lawson, T. and Matthews, J. (2020) ‘Guard Cell Metabolism and Stomatal Function’, *Annual Review of Plant Biology*, 71, pp. 273–302. Available at: https://doi.org/10.1146/annurev-arplant-050718-100251.

Lawson, T. and Vialet-Chabrand, S. (2019) ‘Speedy stomata, photosynthesis and plant water use efficiency’, *New Phytologist*, 221(1), pp. 93–98. Available at: https://doi.org/10.1111/nph.15330.

Long, S.P. *et al.* (2022) ‘Into the Shadows and Back into Sunlight: Photosynthesis in Fluctuating Light’, *Annual Review of Plant Biology*, 73(1), pp. 617–648. Available at: https://doi.org/10.1146/annurev-arplant-070221-024745.

Lowe, D.G. (2004) ‘Distinctive image features from scale-invariant keypoints’, *International journal of computer vision*, 60, pp. 91–110.

Lthi, B.S. *et al.* (2010) ‘An efficient autofocus algorithm for a visible microscope on a Mars lander’, *Planetary and Space Science*, 58(10), pp. 1258–1264. Available at: https://doi.org/10.1016/j.pss.2010.05.002.

McAusland, L. *et al.* (2016) ‘Effects of kinetics of light-induced stomatal responses on photosynthesis and water-use efficiency’, *The New phytologist*, 211(4), pp. 1209–1220. Available at: https://doi.org/10.1111/nph.14000.

Nadal, M. and Flexas, J. (2019) ‘Variation in photosynthetic characteristics with growth form in a water-limited scenario: Implications for assimilation rates and water use efficiency in crops’, *Agricultural Water Management*, 216(August 2017), pp. 457–472. Available at: https://doi.org/10.1016/j.agwat.2018.09.024.

Novick, K.A. *et al.* (2016) ‘The increasing importance of atmospheric demand for ecosystem water and carbon fluxes’, *Nature Climate Change*, 6(11), pp. 1023–1027. Available at: https://doi.org/10.1038/nclimate3114.

Pantaleno, R. *et al.* (2024) ‘Analysis of Guard Cell Readouts Using Arabidopsis thaliana Isolated Epidermal Peels’, *Bio-protocol*, 14(14). Available at: https://doi.org/10.21769/BioProtoc.5033.

Papanatsiou, M. *et al.* (2019) 'Optogenetic manipulation of stomatal kinetics improves carbon assimilation, water use, and growth', *Science*, 363(6434), pp. 1456–1459. Available at: https://doi.org/10.1126/science.aaw0046.

Pattey, E. *et al.* (1991) *Estimation of the net CO2 assimilation rate of a maize (Zea mays L.) canopy from leaf chamber measurements**, *Agricultural and Forest Meteorology*.

Peak, D. (2023) 'Stomatal patchiness and cellular computing', *PNAS*, pp. 1–7.

Reza, A.M. (2004) 'Realization of the contrast limited adaptive histogram equalization (CLAHE) for real-time image enhancement', *Journal of VLSI signal processing systems for signal, image and video technology*, 38, pp. 35–44.

Sai, N. *et al.* (2023) 'StomaAI: an efficient and user-friendly tool for measurement of stomatal pores and density using deep computer vision', *New Phytologist*, 238(2), pp. 904–915. Available at: https://doi.org/10.1111/nph.18765.

Sakoda, K. *et al.* (2021) 'Stomatal, mesophyll conductance, and biochemical limitations to photosynthesis during induction', *Plant Physiology*, 185(1), pp. 146–160. Available at: https://doi.org/10.1093/PLPHYS/KIAA011.

Sezgin, M. and Sankur, B. (2004) 'Survey over image thresholding techniques and quantitative performance evaluation', *Journal of Electronic Imaging*, 13(1), pp. 146–165. Available at: https://doi.org/10.1117/1.1631316.

Vialet-Chabrand, S., Dreyer, E. and Brendel, O. (2013) 'Performance of a new dynamic model for predicting diurnal time courses of stomatal conductance at the leaf level', *Plant, Cell and Environment*, 36(8), pp. 1529–1546. Available at: https://doi.org/10.1111/pce.12086.

Weyers, J.D.B. and Travis, A.J. (1981) *Selection and Preparation of Leaf Epidermis for Experiments on Stomatal Physiology*, *Source: Journal of Experimental Botany*. Available at: https://www.jstor.org/stable/23690065.

Zhang, N. *et al.* (2022) 'Variation of Photosynthetic Induction in Major Horticultural Crops Is Mostly Driven by Differences in Stomatal Traits', *Frontiers in Plant Science*, 13(April), pp. 1–19. Available at: https://doi.org/10.3389/fpls.2022.860229.

Zhang, N. *et al.* (2024) 'Biochemical versus stomatal acclimation of dynamic photosynthetic gas exchange to elevated CO2 in three horticultural species with contrasting stomatal morphology', *Plant*

Cell and Environment [Preprint]. Available at: https://doi.org/10.1111/pce.15043.

[i] Current address Horticulture and Product Physiology, Department of Plant Sciences, Wageningen University & Research, Wageningen 6708PB, The Netherlands

[ii] Current address: Research Institute of Agriculture and Life Sciences, Seoul National University, Seoul, Republic of Korea

Supporting Information to

Viewing stomata in action: Autonomous *in planta* imaging of individual stomatal movement

SM Methods Analyses

Initial processing of the 16 bit images of the z-stacks made per timepoint was performed with the following script in Fiji:

```
inputDir = getDirectory('Choose Input Directory');

outputDir = getDirectory('Choose Output Directory');


listFiles(inputDir);


list = getFileList(inputDir);


function listFiles(dir) {

    list = getFileList(dir);

    for (i=0; i<list.length; i++) {


        setBatchMode(true);

for (i=0; i<list.length; i++) {

  file = dir + list[i];

  open(file);

  title = getTitle();

run("Despeckle", "stack");

run("Remove Outliers...", "radius=2 threshold=50 which=Bright stack");

run("Enhance Contrast...", "saturated=0.3 normalize process_all use");

run("Linear Stack Alignment with SIFT", "initial_gaussian_blur=1.60 steps_per_scale_octave=3
minimum_image_size=64 maximum_image_size=1024 feature_descriptor_size=4
feature_descriptor_orientation_bins=8 closest/next_closest_ratio=0.92 maximal_alignment_error=25
inlier_ratio=0.05 expected_transformation=Rigid interpolate");

saveAs("tiff", dir+title);

close();

  }

setBatchMode(false);
```

```
    }
}
```

The following images provide examples of the changes in part of an image in the first three steps:

1 Original **2 Despeckle** **3 remove outliers** **4 Enhance contrast**

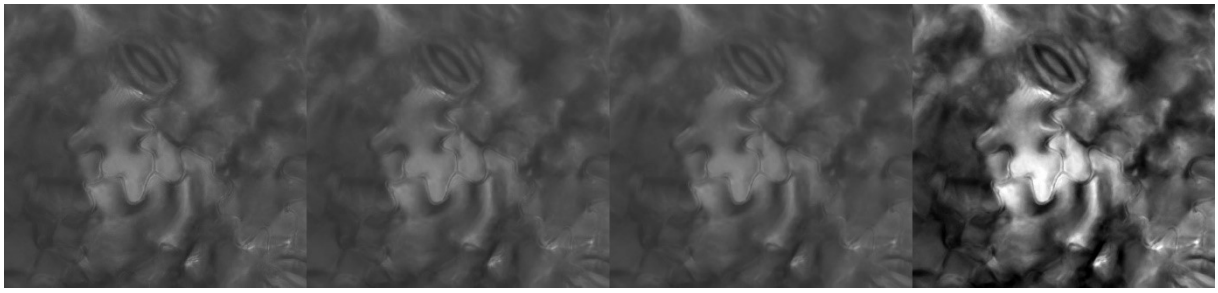

The following graph demonstrates the changes in intensity (Gray value) from these images for the sum of the columns of pixels on the y-axis (Distance (Pixels) describes the x-axis).

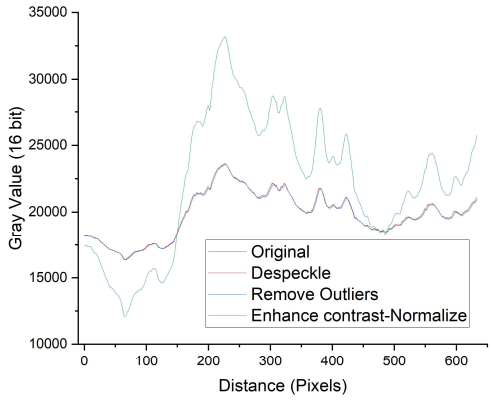

After alignment, stacks of images from individual timepoints were processes with the following script in Fiji:

```
import os, platform

import time

from ij import IJ, WindowManager

from ij.gui import GenericDialog

from ij import IJ, ImagePlus

from ij import IJ

from ij.io import  FileSaver

from loci.plugins.util import BFVirtualStack

from loci.formats import ChannelSeparator

from edfgui import Parameters, ExtendedDepthOfField

Input_Dir = 'DIR'

def walk_through_files(path=str(Input_Dir),file_extension='.tif'):
```

```
        for (dirpath, dirnames, filenames) in os.walk(path):
                for filename in filenames:
                        if filename.endswith(file_extension):
                                yield os.path.join(dirpath, filename)




for fname in walk_through_files():
        print(fname)


        imp = IJ.openImage(fname)
        #imp.show()


        # Create and setup the Parameters object
        param = Parameters()


        # List its attributes or see https://github.com/fiji-BIG/Extended_Depth_Field/blob/6213d53959cef11516a567b3b1120ace4b3e8e07/src/main/java/edfgui/Parameters.java
        # print dir(param)


        # Set projection method
        param.edfMethod = 1    # 0=Sobel, 1=Variance, 2=RealWavelet (default), 3=ComplexWavelet
        #print param.edfMethod
        param.varWindowSize = 5
        #param.daubechielength = 22 # 6,14,22
        #param.nScales = 11 # 1-11
        param.doDenoising = False # True False
        param.reassignment = False # True False
        #param.subBandCC = True # True False
        #param.majCC = True # True False
        #param.sigma = 2
        param.sigmaDenoising = 2
        param.rateDenoising = 10 # 0 to 100%
        param.log = True # True False
```

```
# Create and set up the EDF object
EDF = ExtendedDepthOfField(imp,param)

# Run the projection (can takeseveral seconds depending on the stack size)
# it seems like nothing is happening but the cpu/ram load should increase
EDF.process() # returns void, only display the image

imp = IJ.getImage()


base=os.path.basename(fname)

#print(os.path.dirname(fname))

Dirname = os.path.basename(os.path.dirname(fname))

Base = os.path.splitext(base)[0]

#print(os.path.dirname(fname),Base) # Dit geeft de naam van de sub-map
print('testforsave')
FileSaver(imp).saveAsTiff(os.path.dirname(fname) +'-'+ Base + '.tif')
print('save succesvol')
imp.close()
```

Shade correction with the Pseudo flat field correction of the extended depth of field output (32bit) images was performed with the following script:

```
run("16-bit");
run("Pseudo flat field correction", "blurring=50 hide stack");
```

Contrast enhancement of the Pseudo Flat Field correction output images was performed with the CLAHE algorithm in the following Fiji script:

```
blocksize = 50;
histogram_bins = 256;
maximum_slope = 3;
mask = "*None*";
fast = true;
```

```
process_as_composite = true;


getDimensions( width, height, channels, slices, frames );
isComposite = channels > 1;
parameters =
 "blocksize=" + blocksize +
 " histogram=" + histogram_bins +
 " maximum=" + maximum_slope +
 " mask=" + mask;
if ( fast )
 parameters += " fast_(less_accurate)";
if ( isComposite && process_as_composite ) {
 parameters += " process_as_composite";
 channels = 1;
}


for ( f=1; f<=frames; f++ ) {
 Stack.setFrame( f );
 for ( s=1; s<=slices; s++ ) {
  Stack.setSlice( s );
  for ( c=1; c<=channels; c++ ) {
   Stack.setChannel( c );
   run( "Enhance Local Contrast (CLAHE)", parameters );
  }
 }
}
```

Auto thresholding of fully processed images (e.g. Fig. 3C) is done with the followings scripts in Fiji

Chrysanthemum:

```
run("Auto Threshold", "method=Percentile white show stack");
```

Maize:

```
run("Auto Local Threshold", "method=Bernsen radius=25 parameter_1=0 parameter_2=0 white stack");
```

Lighting and imaging protocols

To fully characterize photosynthetic induction, it is important to reach a steady-state in photosynthesis and stomatal conductance at a given light intensity before switching to a higher light intensity. However, individual stomata often open or close when bulk stomatal conductance is in a steady state. Because we could not measure gas exchange simultaneously with aperture, we were unable to determine whether stomatal conductance was in a steady state. Therefore, we took the times to steady state (see below) from literature (McAusland et al., 2016; Zhang et al., 2022).

Chrysanthemum (shade-sun-shade, 180 min)

Leaves were acclimated to 50 µmol m^{-2} s^{-1} blue-red light and 50 µmol m^{-2} s^{-1} green imaging light for 60 minutes before image acquisition was started. Image stacks were acquired every minute for 120 minutes. After 30 (90 total) minutes, the light intensity was increased to 1000 µmol m^{-2} s^{-1} by increasing the blue-red light intensity to 950 µmol m^{-2} s^{-1}. After another 60 (150 total) minutes the blue-red light intensity was switched back to 50 µmol m^{-2} s^{-1} (total intensity including green measuring light: 100 µmol m^{-2} s^{-1}) for 30 minutes to trigger stomatal closure.

Chrysanthemum (shade-sun-shade, steady-state, 360 min)

Leaves were acclimated to 50 µmol m^{-2} s^{-1} blue-red light and 50 µmol m^{-2} s^{-1} green imaging light for 60 minutes before image acquisition was started. Image stacks were acquired every minute for 300 minutes. After 60 (120 total) minutes, the light intensity was increased to 1000 µmol m^{-2} s^{-1} by increase of the blue-red light intensity to 950 µmol m^{-2} s^{-1}. After another 180 (300 total) minutes, the blue-red light intensity was switched back to 50 µmol m^{-2} s^{-1} (total intensity including green measuring light: 100 µmol m^{-2} s^{-1}) for 60 minutes to trigger stomatal closure.

Maize (growth light - saturating light - growth light, 180 min)

Leaves were acclimated to 425 µmol m^{-2} s^{-1} blue-red light and 75 µmol m^{-2} s^{-1} green imaging light for 60 minutes before image acquisition was started. Image stacks were acquired every minute for 120 minutes. After 30 (90 total) minutes (Period I), the light intensity was increased to 1500 µmol m^{-2} s^{-1} by increase of the blue-red light intensity to 1425 µmol m^{-2} s^{-1} (Period II). After 60 (150 total) minutes the blue-red light intensity was switched back to 425 µmol m^{-2} s^{-1} (total intensity including green measuring light: 500 µmol m^{-2} s^{-1}) for 30 minutes to trigger stomatal closure (Period III).

Table 1 Glossary

SS	Steady-state
QSS	Quasi-steady-state
$A_{0\text{-}i}$	The stomatal aperture at initial SS (μm^2)
A_{max}	The maximum stomatal aperture at the final SS after opening (μm^2)
λ_i	The time lag of the opening response (min)
k_i	The opening time constant (min), a measure of the rapidity of the opening response to SS
Max dAdt-i	Maximum opening speed ($\mu m^2 min^{-1}$)
$A_{0\text{-}d}$	The stomatal aperture at the start of the closing response (μm^2)
$A_{min\text{-}d}$	The final SS or QSS after closing (μm^2)
λ_d	The time lag of the closing response (min)
k_d	The closing time constant (min), a measure of the rapidity of the closing response to SS
Max dAdt-d	Maximum closing speed ($\mu m^2 min^{-1}$)
GCL	Guard Cell Length (µm)
Voronoi area	The leaf area with the shortest path length to a given stoma (μm^2)
FWHM	Full width at half maximum
LED	Light emitting diode
PAR	Photosynthetically active radiation
FOV	Field of View
WUE	Water-Use-Efficiency
NA	Numerical Aperture
VPD	Vapor-pressure-deficit
CLAHE	Contrast limited adaptive histogram equalization

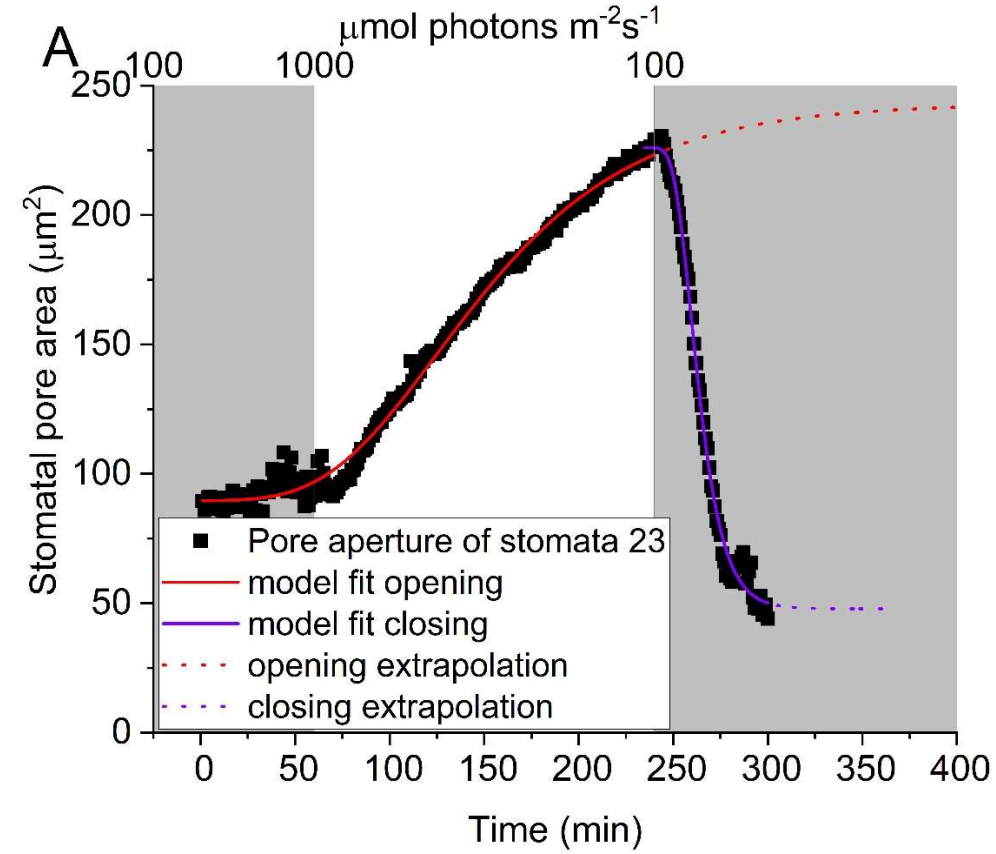
A
µmol photons m-2s-1
100
1000
100
Stomatal pore area (µm2)
Pore aperture of stomata 23
model fit opening
model fit closing
opening extrapolation
closing extrapolation
Time (min)

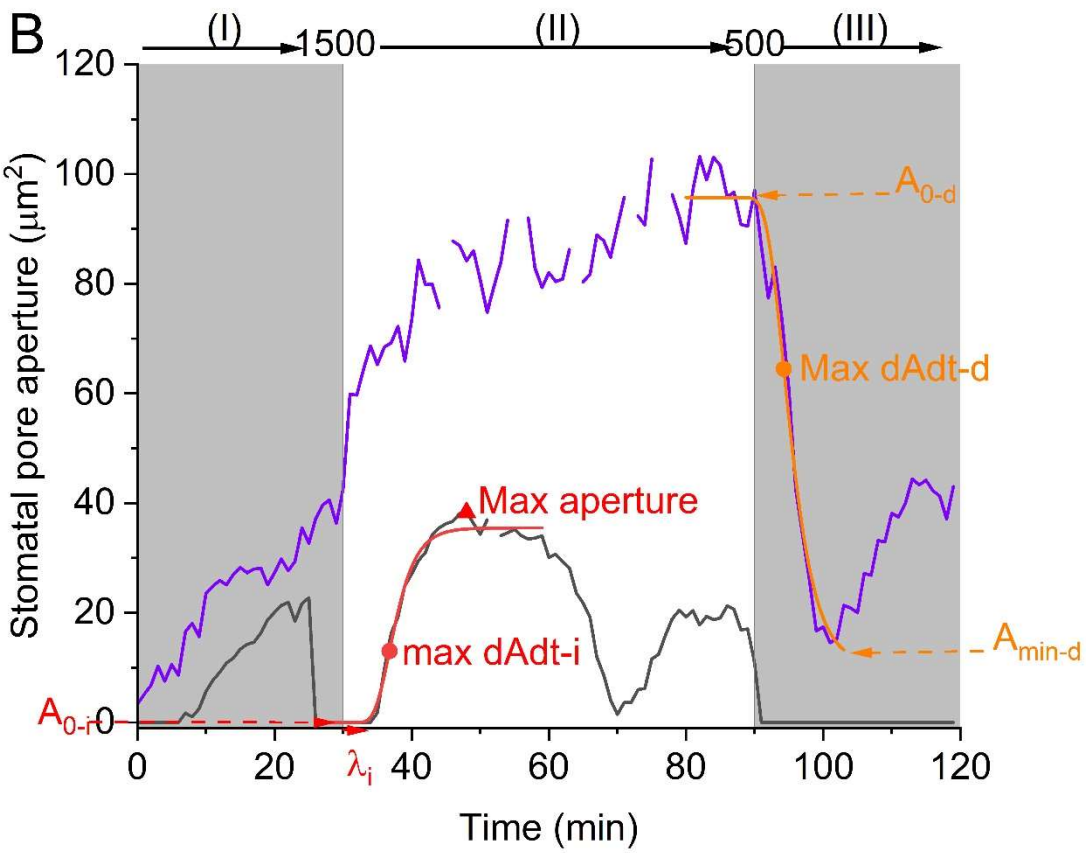
B
(I)
1500
(II)
500
(III)
Stomatal pore aperture (µm2)
A0-d
Max dAdt-d
Max aperture
max dAdt-i
Amin-d
A0-i
λi
Time (min)

SM Fig 1. **A** Example of stomatal aperture dynamics of a single stoma of Chrysanthemum and the model fit for opening (t=60-240) and closing (t=240-300). Black symbols show raw data, and model fits are shown in red/purple. **B** Examples of maize Stomatal dynamics after a change from growth light intensity (500 µmol photons $m^{-2}s^{-1}$) to saturating light intensity (1500 µmol photons $m^{-2}s^{-1}$) and back to growth light intensity. Stoma classified as oscillating between open and closed state (I), opening and oscillating (II) and closing to steady-state (III) is shown in black. Stoma classified as open (I), opening towards new steady-state (II) and closing and oscillating (III) is shown in purple. Examples of opening and closing fit, fit parameters, maximum aperture and time position of the maximum opening and closing speeds are indicated (red: opening, orange: closing).

SM Fig 2 Influence of green imaging light on photosynthesis and stomatal conductance

Green light can reduce the stomatal aperture component driven by blue light at low light intensities (Talbott *et al.*, 2002, 2006). To investigate the effect of green imaging light in combination with red and blue light compared to only red-blue light (RB) typically used for photosynthetic induction experiments on stomatal conductance (gsw) and net photosynthesis rate (A), we used our microscopy light sources in an open top gas exchange system (Li-6800, Li-Cor Biosciences). Cuvette size was 3x3 cm^2, CO_2 was set to 400 µmol mol^{-1}, flow was 400 µmol s^{-1}, air temperature was 25°C, leaf-to-air VPD was 1.06 ± 0.1 kPa (70% relative air humidity). Data were logged every 30 s with 10 s averaging per timepoint. Temperature of the measurement room was 23±1°C, room RH was 70±5% and room [CO_2] was ambient. The light spectrum was switched from RB to red-green-blue light (RGB) with approximately the same total light intensity, after reaching a steady state in ~100 or 95% of steady-state gsw at ~1100 µmol photons $m^{-2}s^{-1}$ in a Chrysanthemum leaf. Green light intensity was 50 µmol $m^{-2}s^{-1}$, and total light intensity was ~100 or ~1100 µmol $m^{-2}s^{-1}$.

In low light, switching from RB in the steady state to RGB (G:RB ratio 1:1) quickly reduced A (to a very small extent), whereas gsw was reduced more slowly and strongly (within 34 min (97% of steady-state in RGB). In contrast, no differences were observed in high light, when switching from RGB (G:RB ratio 0.05:1) to RB back to RGB, corroborating previous research (Talbott *et al.*, 2002, 2006). In conclusion, the apertures observed in our experiments in low light are smaller than those in the typical RB light used for photosynthetic induction due to the decreasing effect of the green imaging light on stomatal aperture.

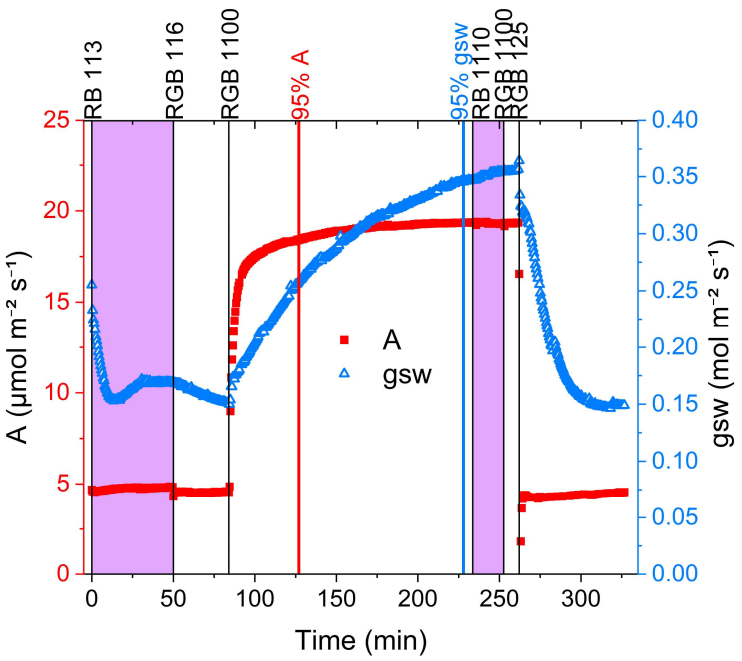

SM Fig. 2 Effect of green imaging light on stomatal conductance and photosynthetic assimilation at 100 and 1100 µmol photons m^2s^{-1}, as measured on a leaf of Chrysanthemum. Stomatal conductance (gsw, blue symbols) and photosynthetic assimilation (A, red symbols) during changes in light spectrum and light intensity are shown. Black vertical lines indicate a change in light spectrum or intensity. Purple areas indicate time period with RB light, white areas indicate time periods with RGB light. Colored vertical lines indicate time-points were 95% of steady-state photosynthetic assimilation (red) or stomatal conductance (blue) are reached.

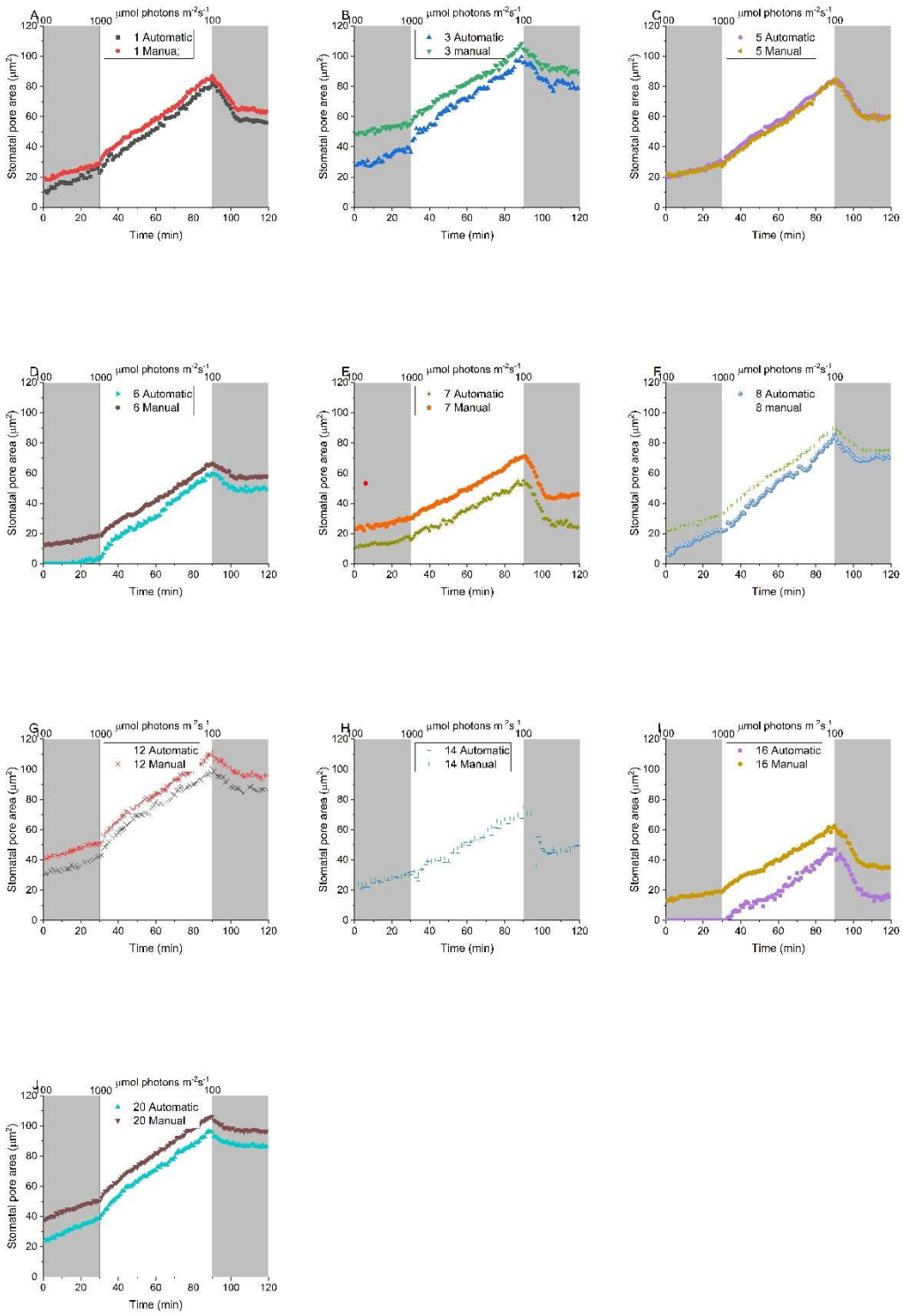

SM Fig. 3. Stomatal aperture dynamics of Chrysanthemum of focus projection images (automatic) and manually determined best single focus images (manual) demonstrating their correlation for 10 individual stomata (A-H)

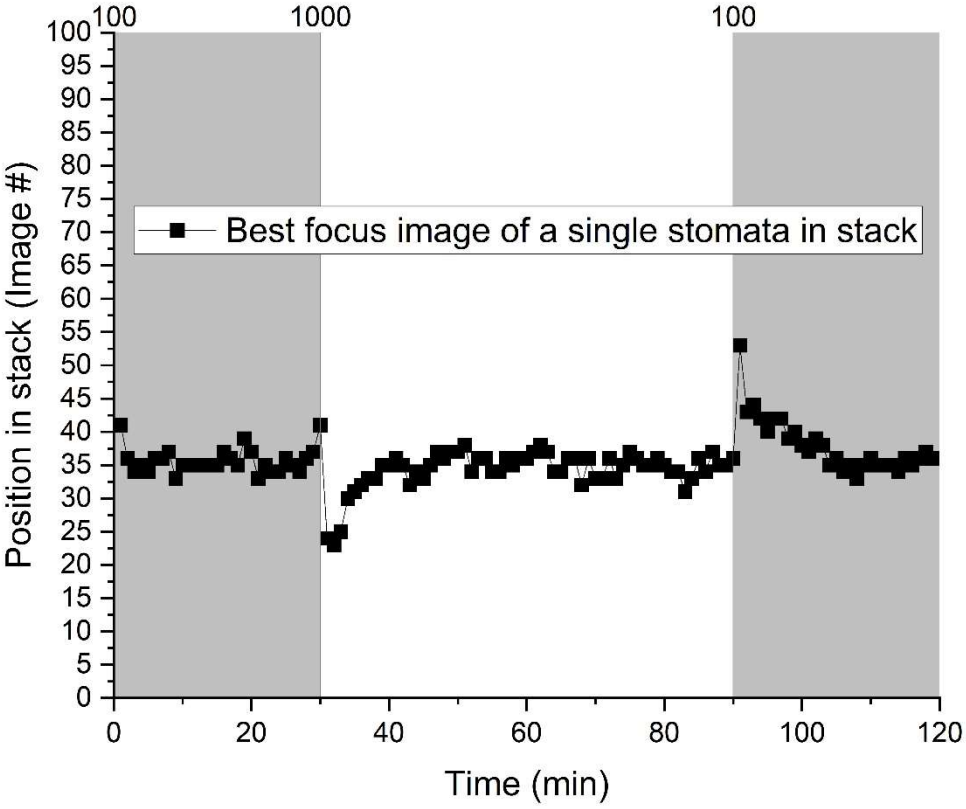

SM Fig. 4 Example of how the position of the best focus for a stoma can change in a stack during the shade-sun-shade experiment in Chrysanthemum due to movement of the leaf surface (Fig. 5).

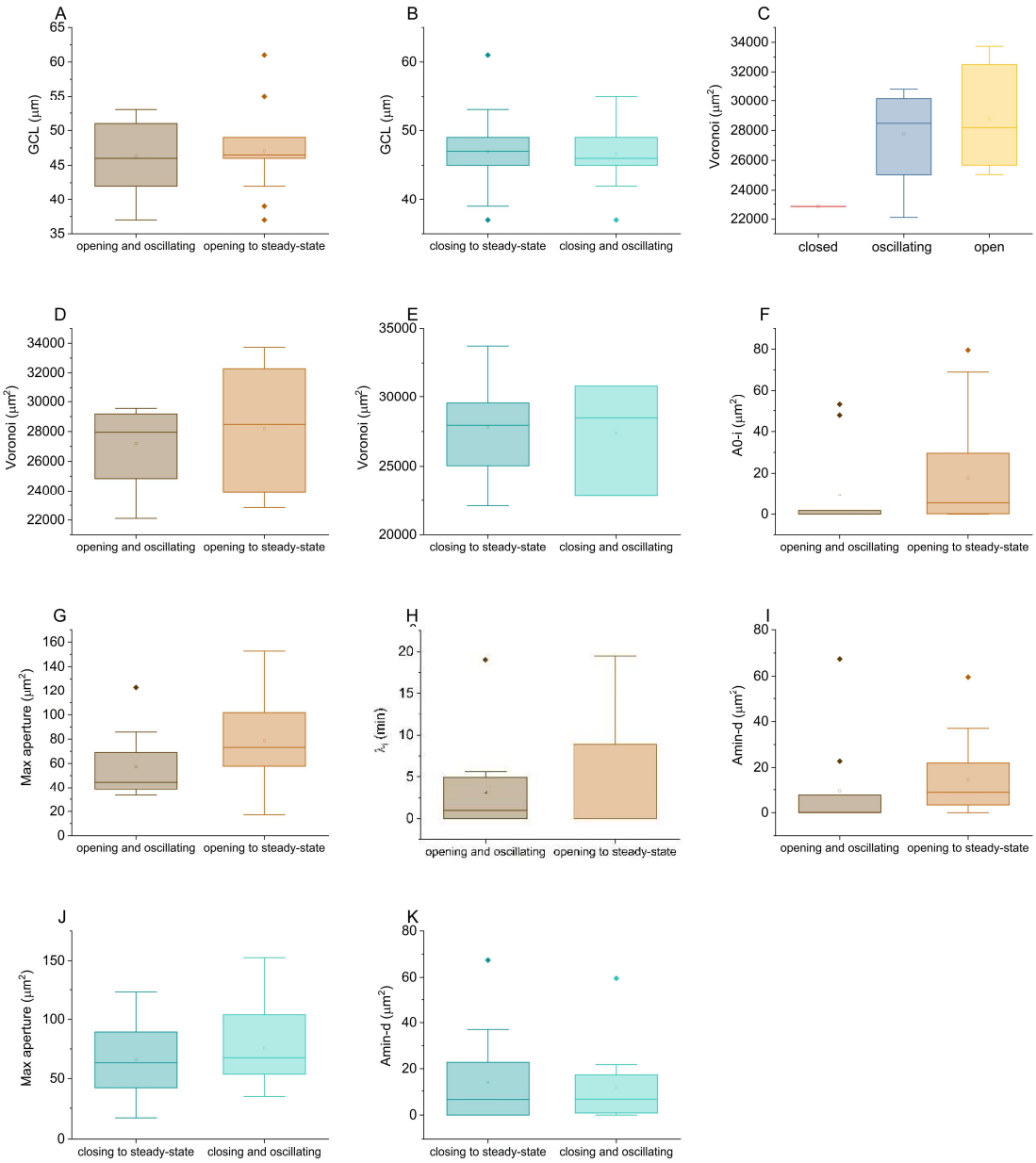

*SM Fig 5. Non-significant differences in comparison of fit and morphological parameters between different categories of Maize stomata tested by ANOVA (AB) or KWANOVA (SW test rejected normality, C-K). Guard Cell length for **A** period II **B** period III. Voronoi area for **C** period I **D** period II **E** period III. **F** Initial, **G** maximum, **I** final aperture and **H** opening lag (λ_i). **J** maximum and **K** final aperture for period III. Squares represent the average and lines the median (Q2). Box outlines represent the lower (Q1) and upper quartile (Q3) and the whiskers indicate Q0 and Q4.*

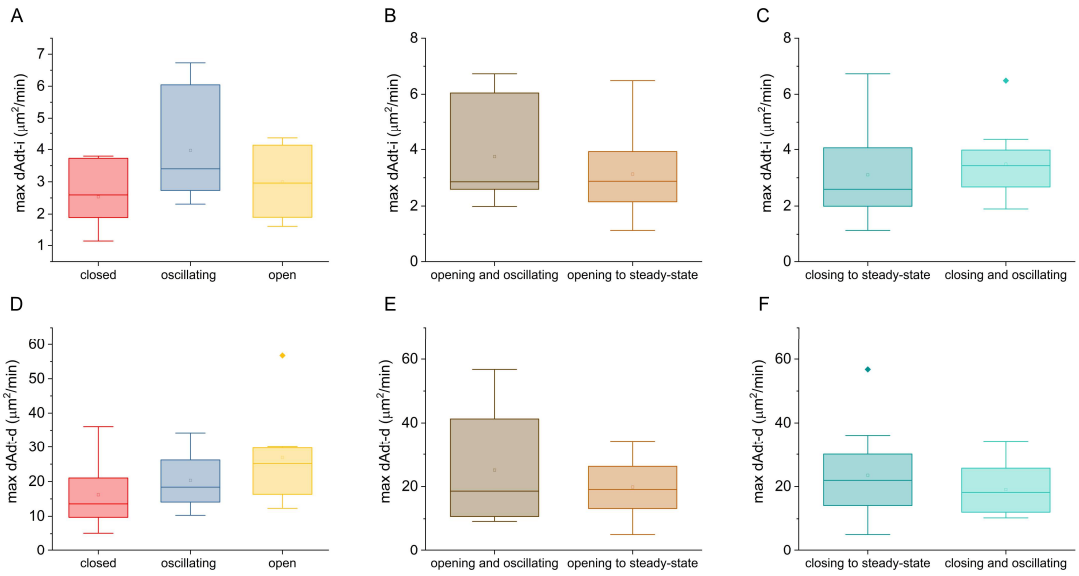

*SM Fig 6. Non-significant differences in comparison of Maize stomatal pore opening (period II) and closing (period III) speeds between different categories tested by KWANOVA (SW test rejected normality). Maximum pore opening speed in period II for category in **A** period I **B** period II **C** period III. Maximum pore closing speed in period III for category in **D** period I **E** period II **F** period III. Squares represent the average and lines the median (Q2). Box outlines represent the lower (Q1) and upper quartile (Q3) and the whiskers indicate Q0 and Q4.*

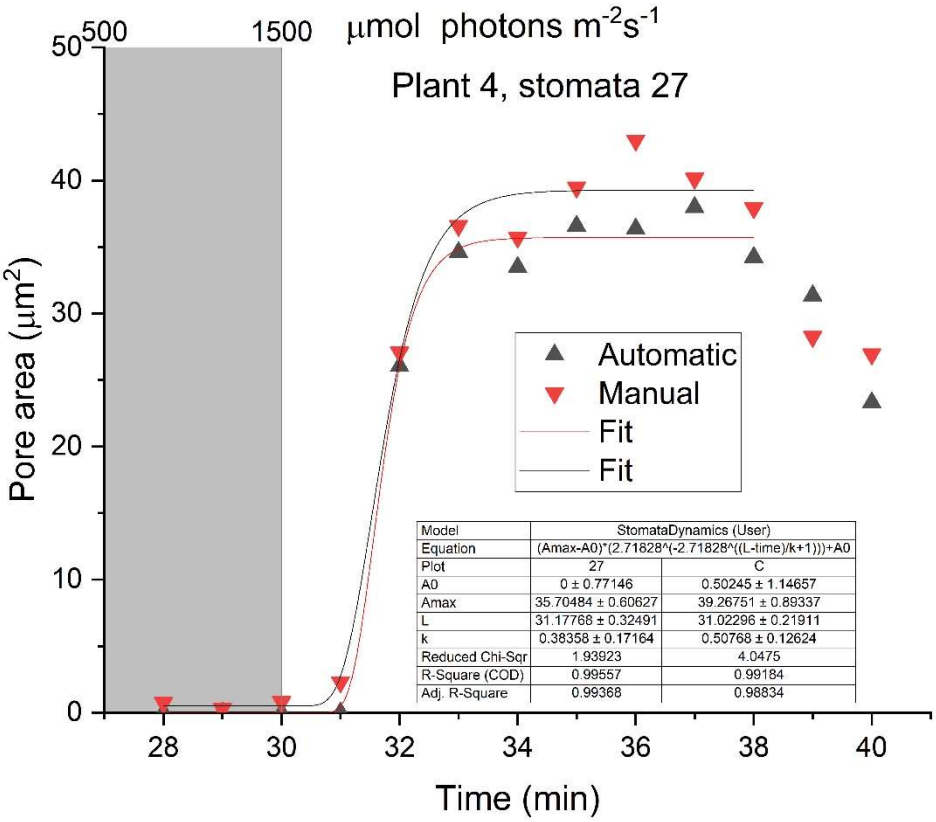

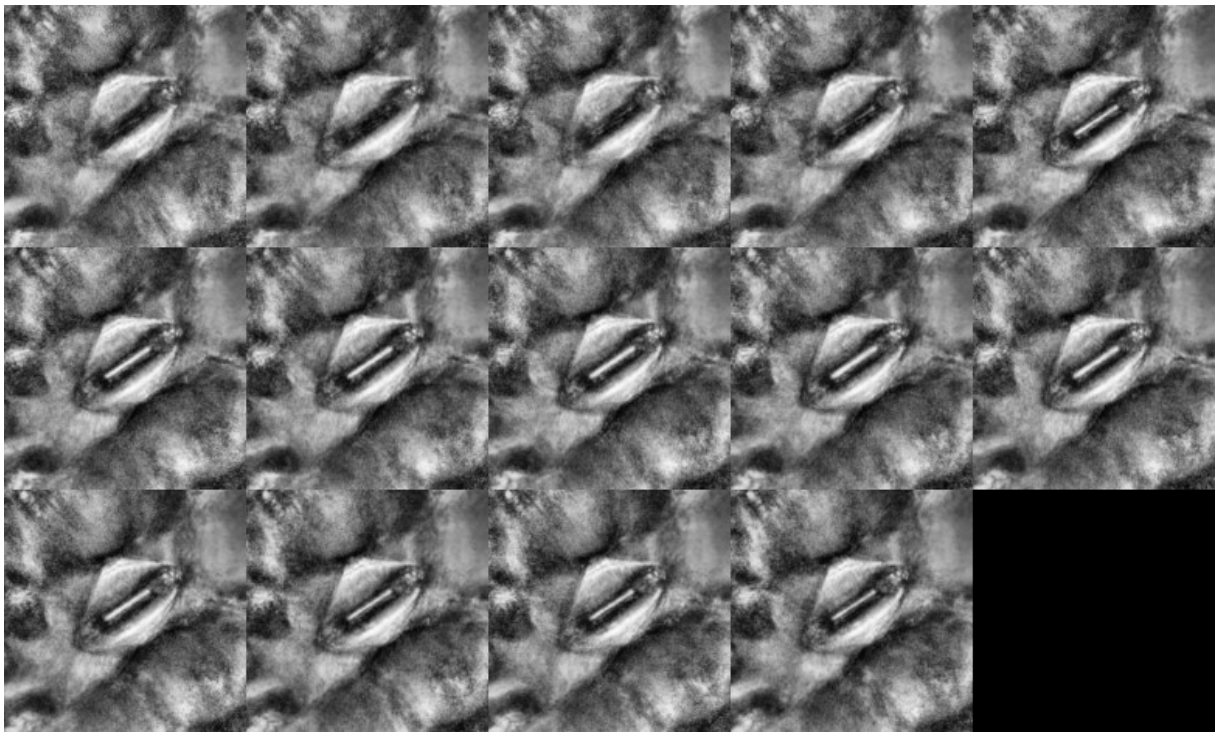

SM Fig. 7 Illustration of large stomatal pore area increase in Maize within a single time-step (<1 min). Timepoints 28 to 41 min are depicted from the best focused single images (Manual, from left to right and top to bottom). Model fits indicate similar results for automatic and manual fits, but both have a large relative error of the fit for the k_i parameter.

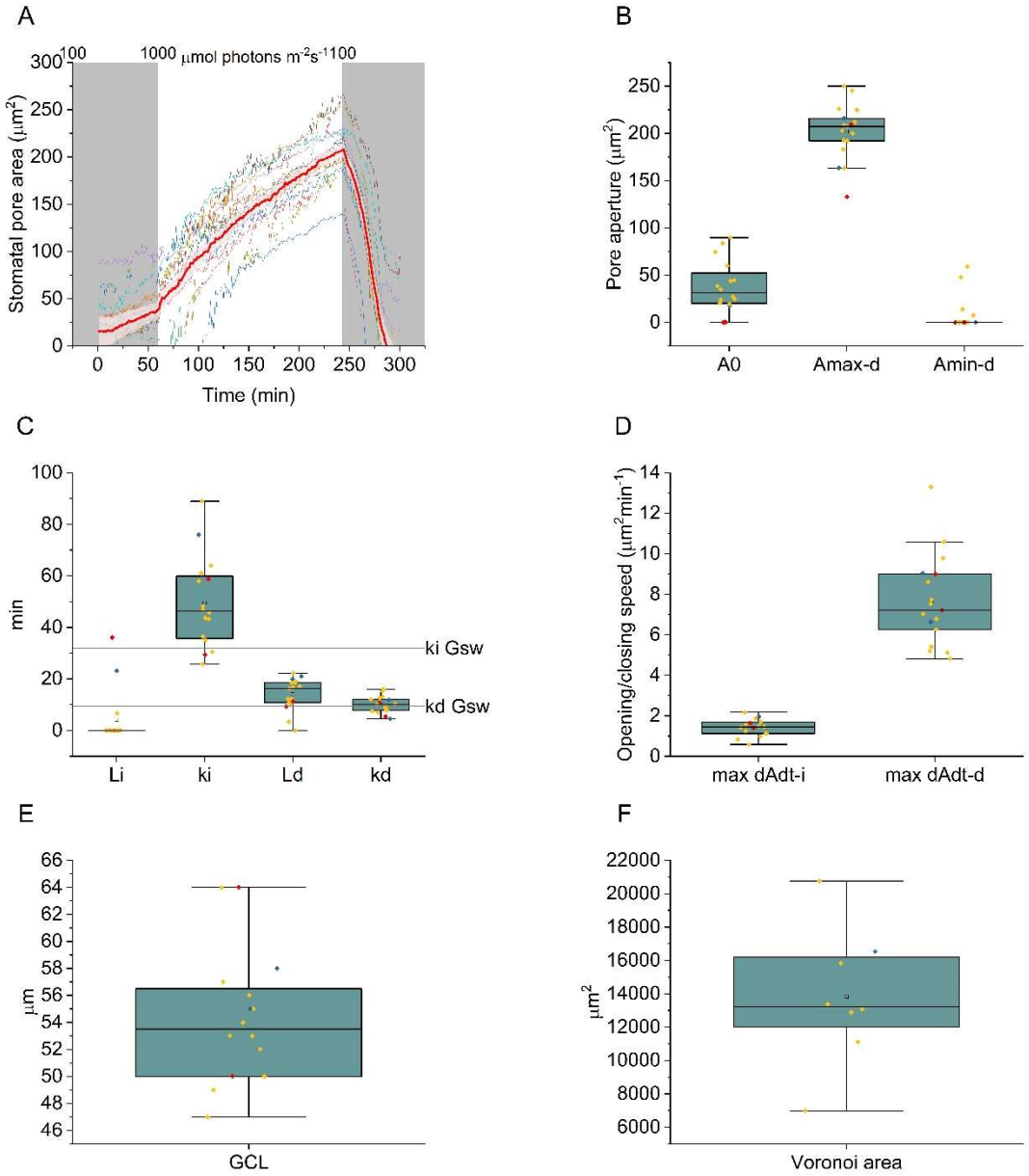
A
100
1000 µmol photons m-2s-1
100
Stomatal pore area (µm2)
Time (min)
B
Pore aperture (µm2)
A0
Amax-d
Amin-d
C
min
ki Gsw
kd Gsw
Li
ki
Ld
kd
D
Opening/closing speed (µm2min-1)
max dAdt-i
max dAdt-d
E
µm
GCL
F
µm2
Voronoi area

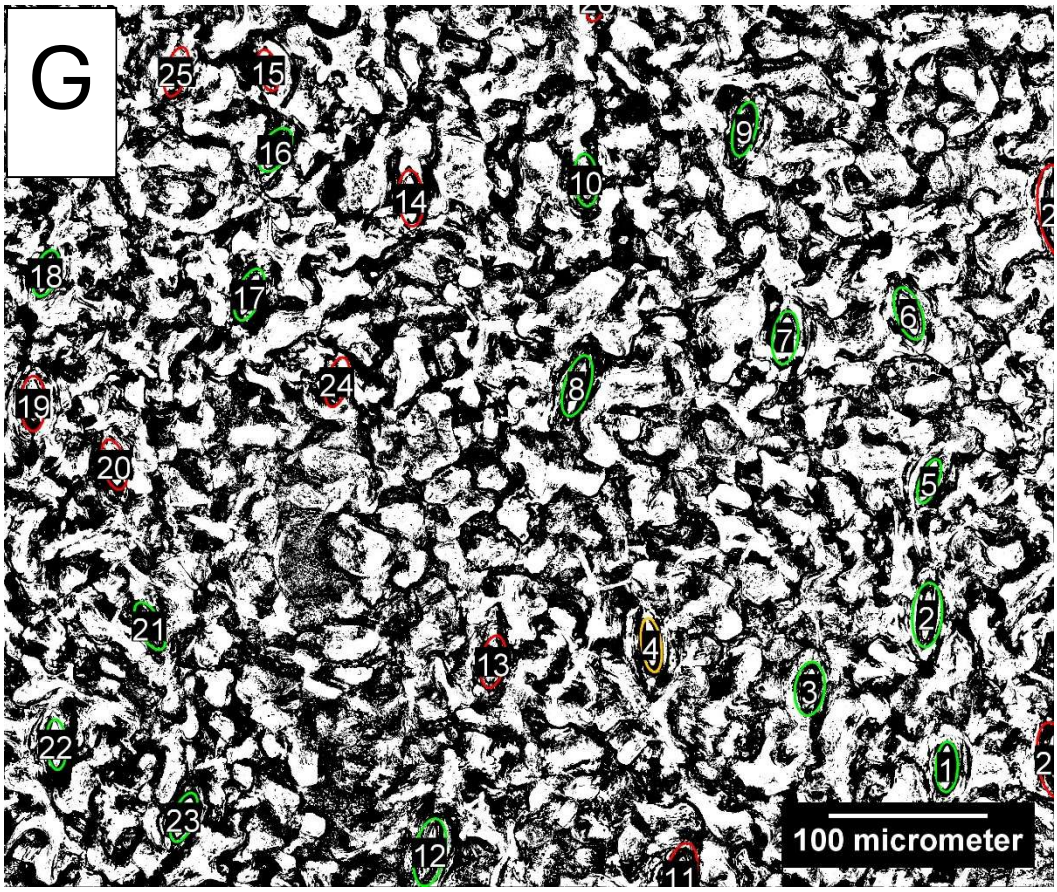

*SM Fig. 8 Induction towards steady-state aperture for individual Chrysanthemum stomata **A** traces for all kinetically resolved stomata (17/28) with their average plotted in red. The shaded red area represents the standard error of the mean. Out of the nine unresolved stomata four were on the image edges and three were shaded by a trichome. For the other two there was no clear indication for the poor segmentation of their pores. Out of the 17 resolved stomata two were closed, two were closing and 13 were opening, both without oscillations, during the sixty minutes of low light. In high light all stomata were increasing towards a steady-state without oscillations. In subsequent low light all stomata decreased to a steady-state without oscillations. **B** Initial, maximum and final apertures fitted parameters on the traces in A **C** fitted time constants of opening (k_i), closing (k_d) as well as fitted opening (λ_i) and closing (λ_d) lag. Horizontal lines represent k_i and k_d determined in gas exchange (SM Fig. 2). **D** maximum pore opening and closing speed. **E** Guard cell length. **F** Voronoi area **B-F** Color of the data points indicates initial opening (yellow), closing (blue) or closed (red) state of the stoma in low light. **G**. Image of the stomata on the epidermis with the oval shapes enclosing the pore are of the stomata. Green stomata were kinetically resolved, orange only resolved for closing and red unresolved. Squares represent the average and lines the median (Q2). Box outlines represent the lower (Q1) and upper quartile (Q3) and the whiskers indicate Q0 and Q4.*

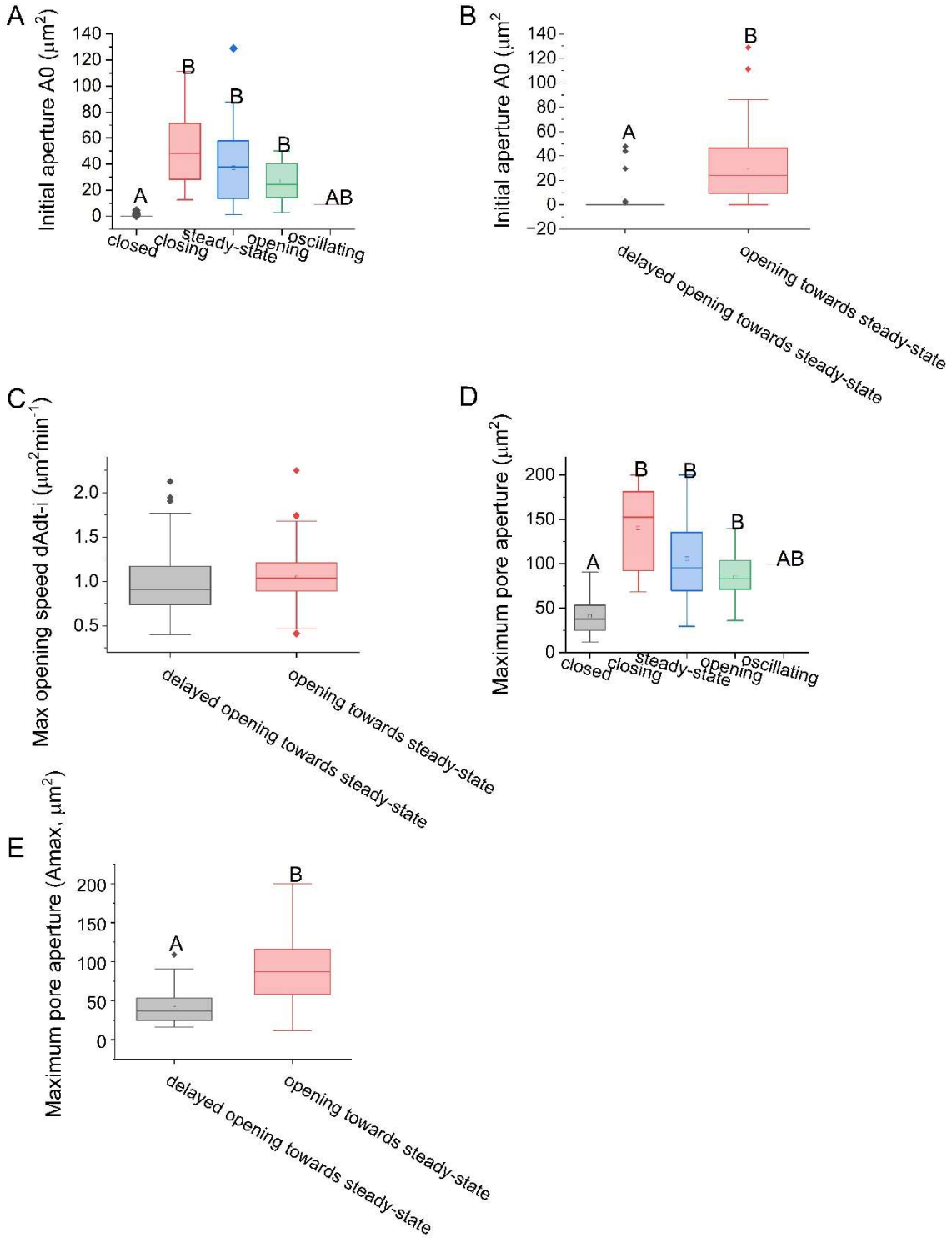

SM Fig. 9. Comparison of kinetic parameters of categorized Chrysanthemum stomata during a shade-sun-shade transition.

A Initial and **D** maximum pore area of the sun shade phase compared between the kinetic categories of the initial shade phase. Number of stomata per category: 47 closed, 25 open in a steady-state, 27 opening, 21 closing and one stoma was open but oscillating. **B** Initial pore

aperture , **C** maximum pore opening speed and **E** Maximum pore aperture in the sun phase compared between the kinetic categories of the sun phase. Number of stomata per category: 87 opening towards steady-state. 37 Delayed opening towards steady-state. Squares represent the average and lines the median (Q2. Box outlines represent the lower (Q1) and upper quartile (Q3) and the whiskers indicate Q0 and Q4.

SM Movie 1 Example of a processed z-stack (100images) of a single timepoint in the shade-sun-shade experiment of Chrysanthemum. Stomatal positions are indicated by red ovals.

SM movie 2 Example of the processed time stack (video) of a complete experiment (119 focus projections of the z-stacks of each timepoint) in the shade-sun-shade experiment of Chrysanthemum. Stomatal positions are indicated by red ovals.

SM video 3 Example of the processed time stack (video) of a complete shade-sun-shade experiment of Chrysanthemum, zoomed in on a single stoma.

SM video 4 The same video of 3 after thresholding.

SM video 5 The same video as 3 and 4 after segmentation.

McAusland, L., Vialet-Chabrand, S., Davey, P., Baker, N. R., Brendel, O., & Lawson, T. (2016). Effects of kinetics of light-induced stomatal responses on photosynthesis and water-use efficiency. *The New Phytologist*, *211*(4), 1209–1220. https://doi.org/10.1111/nph.14000

Zhang, N., Berman, S. R., Joubert, D., Vialet-Chabrand, S., Marcelis, L. F. M., & Kaiser, E. (2022). Variation of Photosynthetic Induction in Major Horticultural Crops Is Mostly Driven by Differences in Stomatal Traits. *Frontiers in Plant Science*, *13*(April), 1–19. https://doi.org/10.3389/fpls.2022.860229